HHS Public Access

Author manuscript

Cancer Cell. Author manuscript; available in PMC 2024 January 23.

Published in final edited form as:

Cancer Cell. 2020 May 11; 37(5): 705–719.e6. doi:10.1016/j.ccell.2020.03.004.

A deregulated HOX gene axis confers an epigenetic vulnerability in *KRAS*-mutant lung cancers

Stephanie L. Guerra[1,2], **Ophélia Maertens**[1,2], **Ryan Kuzmickas**[1,2], **Thomas De Raedt**[1,2], **Richard O. Adeyemi**[1,2], **Caroline J. Guild**[1,2], **Shawna Guillemette**[1,2], **Amanda J. Redig**[3], **Emily S. Chambers**[3], **Man Xu**[4], **Hong Tiv**[5], **Sandro Santagata**[2,6,7], **Pasi A. Jänne**[2,3,4], **Steve Elledge**[1,7,8,9], **Karen Cichowski**[1,2,7,10,*]

[1]Genetics Division, Department of Medicine, Brigham and Women's Hospital, Boston, MA 02115, USA

[2]Harvard Medical School, Boston, MA 02115, USA

[3]Lowe Center for Thoracic Oncology, Dana Farber Cancer Institute, Boston, 02115, MA

[4]Belfer Center for Applied Cancer Science, Boston, MA 02115, USA

[5]Experimental Therapeutic Core, Dana-Farber Cancer Institute, Boston, Massachusetts, USA.

[6]Departments of Pathology, Brigham and Women's Hospital, Dana Farber Cancer Institute, Boston, Massachusetts, 02115, USA

[7]Ludwig Center at Harvard, Harvard Medical School, Boston, MA 02115, USA

[8]Department of Genetics, Harvard Medical School, Boston, MA 02115, US

[9]Howard Hughes Medical Institute, 77 Avenue Louis Pasteur, Boston, MA 02115, USA.

[10]Lead contact

SUMMARY

While *KRAS* mutations are common in non-small cell lung cancer (NSCLC), effective treatments are lacking. Here we report that half of *KRAS*-mutant NSCLCs aberrantly express the homeobox protein HOXC10, largely due to unappreciated defects in PRC2, which confers sensitivity to combined BET/MEK inhibitors in xenograft and PDX models. Efficacy of the combination is dependent on suppression of *HOXC10* by BET inhibitors. We further show that HOXC10 regulates the expression of pre-replication complex (pre-RC) proteins in sensitive tumors. Accordingly, BET/MEK inhibitors suppress pre-RC proteins in cycling cells, triggering stalled

*Address correspondence to: kcichowski@rics.bwh.harvard.edu; fax (617) 525-4705; phone (617) 525-4722.

AUTHOR CONTRIBUTIONS

Conceptualization, S.G. and K.C.; Methodology, S.G., K.C. and S.J.E.; Formal Analysis, R.K., T.D.R., S.G., O.M., R.O.A.; Investigation, S.G., R.A., S.G., O.M., S.S., H.T., C.G., M.X.; Resources, A.R., E.C., M.X.; Writing-Original Draft, S.G., K.C. and Writing-Re-view & Editing, S.G., K.C., O.M., S.J.E. and P.A.J.

None of these represent competing interests.

replication, DNA damage, and death. These studies reveal a promising therapeutic strategy for *KRAS*-mutant NSCLCs, identify a predictive biomarker of response, and define a subset of NSCLCs with a targetable epigenetic vulnerability.

eTOC blurb

Guerra et al. show that combined MEK and BET inhibitors are effective in ~50% of *KRAS*-mutant NSCLC. HOXC10 is a biomarker of response and regulates expression of pre-replication complex proteins in conjunction with MEK. MEK/BET inhibitors suppress HOXC10 to trigger replication defects and induce cell death.

Graphical Abstract

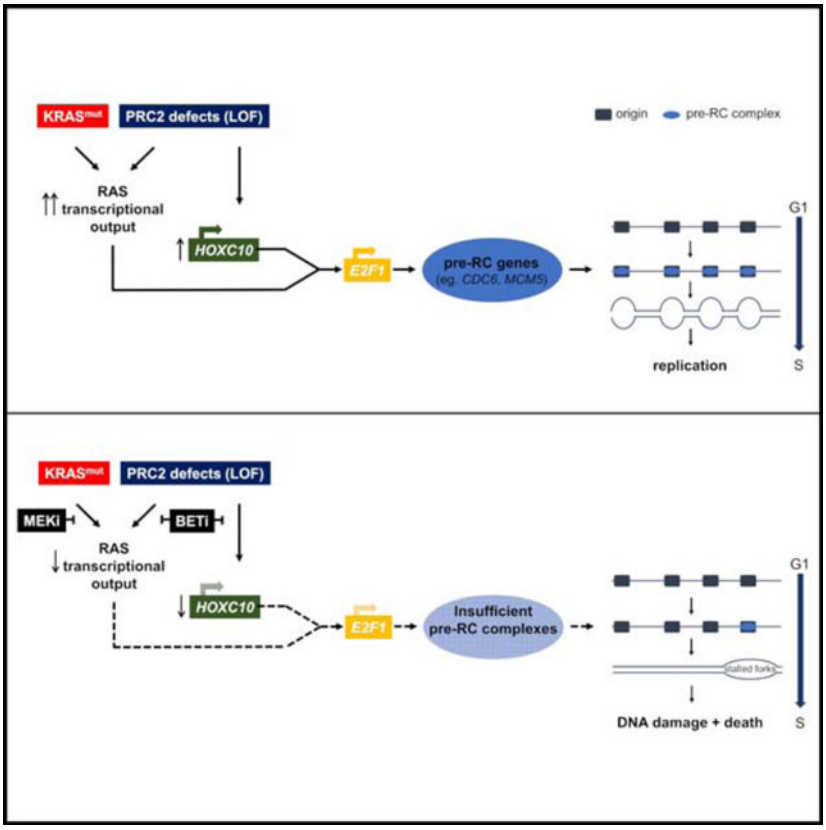

Keywords

KRAS; lung cancer; NSCLC; MEK; BET; HOXC10; combination therapy

INTRODUCTION

Agents that suppress oncogenic kinases have changed the standard of care for many cancers. In NSCLC, kinase inhibitors are routinely used to treat tumors with alterations in *EGFR*, *ALK*, *ROS1* and *MET* (Reck and Rabe, 2017). However, there are no effective therapies for *KRAS*-mutant lung cancers. One strategy has been to target Ras effectors, such as MEK.

Unfortunately, MEK inhibitors exhibit little efficacy as single agents or when combined with chemotherapy (Janne et al., 2017). Covalent KRAS inhibitors have shown promise in preclinical models, although current agents are only effective against a specific mutant allele (Janes et al., 2018; Ostrem et al., 2013; Zeng et al., 2017). Evidence further suggests that these inhibitors will require additional agents for maximal efficacy (Lito et al., 2016; Misale et al., 2019; Patricelli et al., 2016). As such, the identification of effective therapeutic strategies for treating *KRAS*-mutant lung cancers remains an urgent unmet need.

BET proteins bind acetylated histones and recruit transcription factors to active promoters and enhancers. Small molecules that target BET proteins have emerged as potential therapeutic agents (Stathis and Bertoni, 2018). Importantly, BET inhibitors have shown preliminary clinical activity in NUT carcinomas, which are driven by BRD4-NUT translocations (Lewin et al., 2018; Stathis et al., 2016). These agents are also being evaluated in hematopoietic and solid malignancies, often based on the rationale that they suppress MYC (Delmore et al., 2011). However, clinical sensitivity thus far does not appear to be related to MYC expression (Amorim et al., 2016; Berthon et al., 2016; Lewin et al., 2018; Stathis et al., 2016). Therefore, while these observations support the further investigation of BET inhibitors, to develop successful therapies we must better understand their mechanism of action, identify predictive biomarkers, and design more effective drug combinations. Combinatorial approaches are likely to be particularly important for solid tumors lacking BET translocations.

One therapeutic approach for treating Ras pathway-driven tumors, has been to combine agents that cooperatively, and therefore more deeply, suppress ERK signaling. This paradigm underlies the success of BRAF/MEK inhibitors in *BRAF*-mutant melanoma (Flaherty et al., 2012); however, a similar strategy has not been developed for *KRAS*-mutant cancers. Interestingly, BET inhibitors have been shown to attenuate the Ras pathway in *NF1*-mutant tumors, not by affecting signaling but by suppressing Ras-driven transcriptional output (De Raedt et al., 2014). Therefore, we hypothesized that BET inhibitors might enhance the effects of MEK inhibitors in *KRAS*-mutant tumors. Here we deconstruct the unexpected mechanism by which MEK/BET inhibitors kill 50% of *KRAS*-mutant NSCLCs. In addition to identifying a promising therapeutic strategy for these malignancies, these studies have also uncovered a distinct subset of NSCLCs with a tractable epigenetic vulnerability.

RESULTS

MEK/BET inhibitors trigger cell death and tumor regression in *KRAS*-mutant lung adenocarcinomas

KRAS mutations occur in approximately 1/3 of human NSCLCs and *NF1* is mutated in an additional 8.3% (Cancer Genome Atlas Research, 2014). To investigate the therapeutic potential of BET/MEK inhibitors in these cancers, cells harboring *KRAS* or *NF1* mutations were treated with a MEK inhibitor (PD-325901:PD901) and/or a BET inhibitor (JQ1). Both *KRAS*-mutant lines tested were exquisitely sensitive to these agents, which when combined caused a 68–74% decrease in cell number in 72 hours; but these agents were cytostatic, at best, in the *NF1*-mutant cells (Figure 1A). Efficacy was not related to differential effects

on ERK, which was effectively suppressed in all cells (Figure 1A, bottom). In addition, MYC levels were unaffected, suggesting that MYC suppression was not responsible for the response (Figure S1A).

Additional *KRAS*-mutant NSCLCs were screened to assess the frequency of sensitivity. MEK/BET inhibitors caused dramatic cell loss in half of the cell lines (Figure 1B, Figure S1B). Cytostatic responses were observed in the remaining lines, however cells did not die and were therefore termed ‘resistant’. These differential responses were further visualized using live-cell imaging. In sensitive cells, MEK and BET inhibitors alone suppressed proliferation to varying extents, but combined agents triggered a robust and continuous loss of cells, killing the majority of cells within days (Figure 1C, top; Figure S1C). By contrast, in resistant cells single agents also slowed proliferation and together MEK/BET inhibitors exerted potent cytostatic effects; however, these agents did not cause a loss of cells, suggesting that they were unable to trigger cell death (Figure 1C, bottom).

To determine whether sensitive cells were dying via apoptosis, caspase 3/7 activity was measured using live-cell imaging. Combined MEK/BET inhibitors triggered apoptosis in 60–70% of cells within 4 days (Figure 1D, top; Figure S1D). By contrast, combined MEK/BET inhibitors did not induce apoptosis in resistant lines (Figure 1D, bottom). PARP cleavage further confirmed these findings (Figure S1E). Thus, while combined MEK/BET inhibitors exert potent cytostatic effects in resistant cells, they exclusively trigger cell death in sensitive cells.

To examine the durability of the response, long-term colony forming assays were performed. MEK and BET inhibitors individually slowed the proliferation of sensitive cells, demonstrated by a relative reduction in colonies after 1 week (Figure 1E, top). However, differential responses to single agents were no longer apparent in some cell lines after 3 weeks, due to the slow but continuous proliferation of cells (Figure 1E, bottom). By contrast, combined inhibitors exerted a robust cytotoxic response, rapidly eliminating the vast majority, if not all, cells in sensitive lines, which was apparent at 1 and 3 weeks (Figure 1E, F).

Dose-response studies were also performed. Based on IC50 values, sensitive cells were not inherently more sensitive to either agent (Table S1). In addition, a shift in dose-response was readily observed when MEK and BET inhibitors were combined in sensitive cells (e.g. HCC44, H1573), compared to resistant cells (A549, H1373). (Relative IC50 values, Figure 1G; raw values, Figure S1F). As such, IC50 values of combined agents were generally lower in sensitive versus resistant cell lines (Table S2). Nevertheless, IC50 values, which largely measure effects on proliferation, do not accurately reflect the biology of this response. For example, A549 (resistant) cells appear to be the most sensitive to MEK inhibitors as determined by IC50 values (Table S1). However, while MEK inhibitors exerted potent cytostatic effects, they did not trigger death even in the presence of BET inhibitors (Figure 1D) and BET inhibitors did not enhance sensitivity to MEK inhibitors (Figure 1G). By contrast, H1573 and H23 cells, which exhibit combined IC50 values similar to A549 cells, potently died in the presence of combined agents (Figure 1D and Figure S1D). Even at concentrations where agents exerted cooperative cytostatic effects, they failed to kill

resistant cells (Figure 1B, Figure S1G). These observations highlight the need to directly examine cell death and the net loss of cells, to identify combinations that kill rather than enhance cytostatic effects, the former of which is likely to have a greater therapeutic impact.

Therapeutic effects were next evaluated *in vivo*. Agents that slow tumor growth in animal models have been proposed to be promising clinical candidates; however, clinically effective agents invariably cause frank tumor regression (e.g. BRAFi in melanoma, EGFRi in NSCLC). Two xenograft models derived from sensitive lines were generated. Single agents exerted modest cytostatic effects at best, however MEK/BET inhibitors together induced potent tumor regression (Figure 1H-J). Phospho-ERK was effectively suppressed *in vivo* and no toxicity was observed (Figure S2A, B). In addition, these agents did not cause tumor regression in resistant tumors (Figure S2C). Trametinib, an approved MEK inhibitor, and AZD5153, a structurally distinct BET inhibitor currently in clinical trials, triggered similar cytotoxic effects *in vitro* and tumor regression *in vivo* (Figure 1K, L). These data demonstrate that MEK and BET inhibitors potently cooperate *in vitro* and *in vivo* to induce both cell death and frank tumor regression.

Sensitive NSCLCs overexpress the homeobox gene, *HOXC10*

To look for molecular determinants of sensitivity or resistance, mutational and copy number data from CCLE datasets of lines in Figure 1B were evaluated using the cBioPortal visualizer (http://www.cbioportal.org/). This analysis did not reveal mutations, amplifications, or homozygous deletions associated with either group, including alterations in *TP53*, *MYC*, *STK11*, *CDKN2A/B*, and *SMARCA4* (Figure S3A). As an alternative approach, we investigated differentially expressed genes in sensitive versus resistant lines. RNA-seq data from lines in Figure 1B were obtained from the CCLE. A two-class comparison test was used to identify genes differentially expressed between the two groups ($p \leq 0.001$). A similar strategy has been used to identify predictive biomarkers in other settings (Maertens et al., 2019). Only 11 genes were found to be differentially expressed. The average expression of each gene (Figure 2A), and the individual expression of these genes in every cell line (Figure S3B) are shown. Strikingly, the homeobox gene, *HOXC10*, was by far the most differentially upregulated and was exclusively overexpressed in all sensitive lines (Figure 2A, Figure S3B). This pattern of HOXC10 expression was confirmed by Q-PCR and immunoblots, which revealed a dramatic binary difference in expression; HOXC10 was readily detected in sensitive cells but was absent or nearly undetectable in resistant cells (Figure 2B). This observation was intriguing because aberrant expression of *HOX* genes plays a well-established role in cancer, most notably *HOXA9* in AML (Shah and Sukumar, 2010). HOXC10 is overexpressed in some tumor types, although little is known about its potential function (Feng et al., 2015; Sadik et al., 2016). Regardless, these observations demonstrate that HOXC10 marks a distinct set of *KRAS*-mutant NSCLCs that are uniquely sensitive to combined MEK/BET inhibitors.

HOXC10 suppression is required for NSCLC cell death

To elucidate the mechanism of action, transcriptional responses of drug treated cells were examined. Based on our original hypothesis that BET inhibitors might function by further suppressing Ras transcriptional output, we first assessed effects on Ras transcriptional

signatures. Indeed, MEK/BET inhibitors cooperatively suppressed these signatures in sensitive cells (Figure 2C). Surprisingly however, a cooperative suppression of Ras transcriptional signatures was also detected in resistant cells, where only cytostatic responses were observed (Figure S3C). These findings suggest that while enhanced suppression of the Ras transcriptional network likely contributes to cytostasis, it is not sufficient for cell death. Consistent with this notion, *KRAS* ablation in *KRAS*-mutant tumor cells often inhibits proliferation but does not cause cell death (Singh et al., 2009), as observed in our sensitive cells (Figure 2D). Moreover, while the effects of *KRAS* knockdown were potentiated by MEK inhibitors, a full cytotoxic response was only achieved when BET inhibitors were included (Figure 2D). These observations indicate that while BET inhibitors potentiate the suppression of Ras-driven transcriptional output, they must also provide an additional signal for cell death to occur.

Because the only observable difference between sensitive and resistant cells was the aberrant expression of HOXC10, and because the overexpression of specific proteins in cancer often confers a dependency on those proteins (e.g. HER2, MET, HOXA9), we investigated whether MEK/BET inhibitors might function by suppressing HOXC10. Strikingly, BET inhibitors suppressed HOXC10 in sensitive cells and downregulation was sustained in the presence of both agents (Figure 2E). Microarray and Q-PCR analysis further demonstrated that suppression occurred at the level of transcription, consistent with the known function of BET proteins (Figure S3D, E). HOXC10 was also potently suppressed by BET and MEK/BET inhibitors in tumors *in vivo* (Figure 2F). Most importantly, while ectopic HOXC10 expression had no effect on cell proliferation, it completely inhibited death in response to MEK/ BET inhibitors, demonstrated by cell counting (Figure 2G, Figure S3F) and PARP cleavage (Figure 2H). These results demonstrate that HOXC10 suppression is necessary for cell death in response to MEK/BET inhibitors.

To determine whether HOXC10 suppression was sufficient for this response, siRNAs were used to inhibit its expression. Acute loss of HOXC10 had no effect on its own, however HOXC10 suppression killed sensitive cells when combined with MEK inhibitors (Figure 2I). Notably, effects were less potent than those observed in response to combined MEK/BET inhibitors as might be expected, given the enhanced suppression of Ras transcriptional output conferred by BET inhibition (Figure 2I and 2C). Together these findings indicate that HOXC10 is a critical target of BET inhibitors in NSCLCs and that its suppression is both necessary and sufficient to kill cells when combined with MEK inhibitors; however, more profound therapeutic effects are conferred by BET inhibitors, which further suppress Ras/MEK transcriptional output.

Given the functional importance of HOXC10, we sought to further substantiate it as a potential predictive biomarker. Additional *KRAS*-mutant cell lines with either high or low *HOXC10* (CCLE), were prospectively selected for analysis. Notably, those that expressed HOXC10 were sensitive to MEK/BET inhibitors, whereas cells that lacked HOXC10 were not (Figure 2J). Retrospective analysis of the two unresponsive *NF1*-mutant cell lines in Figure 1A demonstrated that these also lacked HOXC10 expression, as would be predicted (Figure 2K). These results suggest that HOXC10 is both a predictive and functional biomarker of sensitivity to MEK and BET inhibitors.

HOXC10 marks a distinct set of NSCLCs and PDX tumors that are sensitive to MEK/BET inhibitors

HOXC10 is overexpressed in 51% of primary *KRAS*-mutant tumors (Figure 3A; TCGA, ≥ 2SD over expression in normal lung), consistent with observations in cell lines (Figure 2B). By analyzing *KRAS*-mutant tumor/normal matched tissue pairs, HOXC10 was found to be specifically overexpressed in tumor tissue in 8/9 of the HOXC10-expressing samples (Figure 3B). To assess efficacy in primary tumors, HOXC10 expression levels were examined in 3 *KRAS*-mutant patient-derived xenograft (PDX) models. Robust HOXC10 expression was observed in 1 PDX model (genotype: *KRAS G12C/TP53 G245V*, DFCI-201), confirmed by both immunoblot and immunohistochemistry (Figure 3C, 3D). Similar to xenografts, combined MEK/BET inhibitors also caused frank tumor regression in these PDX tumors (Figure 3E), underscoring the potential clinical utility of this combination.

PRC2 defects trigger aberrant HOXC10 expression and confer sensitivity to MEK/BET inhibitors

HOX genes are typically expressed during development but can be aberrantly expressed in cancer through a variety of mechanisms (Abate-Shen, 2002; Krivtsov and Armstrong, 2007). In leukemia, HOXA9 expression is frequently driven by translocations. However, HOX genes are normally regulated by Trithorax and PRC2 complexes, which activate and repress HOX genes, respectively (Mallo and Alonso, 2013). A deeper analysis of PRC2 genes revealed that all sensitive *KRAS*-mutant cell lines exhibited single copy loss or mutations in at least one obligate component (*SUZ12*, *EED*, or *EZH2*) whereas resistant lines did not ((Cancer Genome Atlas Research, 2014); Figure 4A). These events were not captured in our initial analysis because different PRC2 genes are affected in different lines. Loss-of-function defects in PRC2 components are prevalent in T-ALL and MPNSTs (De Raedt et al., 2014; Lee et al., 2014; Ntziachristos et al., 2012; Zhang et al., 2014). However, unlike these examples, homozygous loss of PRC2 genes was not detected in *KRAS*-mutant lung cancers (Cancer Genome Atlas Research, 2014). Nevertheless, ssGSEA analysis confirmed that PRC2 targets were upregulated (de-repressed) in sensitive lines, suggesting that heterozygous cells exhibit functional defects in PRC2 (Figure 4B). PRC2 transcriptional signatures were also de-repressed in primary NSCLCs with heterozygous loss of PRC2 components, as compared to those with intact PRC2 genes (p=0.01) (Figure S4A).

HOX genes are canonical PRC2 targets (Schuettengruber et al., 2017) and HOXC10 is a direct PRC2 target, as demonstrated by ChIP-X Enrichment Analysis and ENCODE datasets (Rouillard et al., 2016). Nevertheless, to confirm that 1) HOXC10 is regulated by the PRC2 in NSCLCs and that 2) defects in PRC2 components are responsible for conferring sensitivity to MEK/BET inhibitors through effects on HOXC10, *SUZ12* or *EED* shRNA sequences were introduced into resistant cells. Suppression of either PRC2 component triggered the expression of HOXC10 (Figure 4C). Moreover, shRNA-mediated inhibition of *SUZ12* or *EED* expression caused resistant cell lines to become sensitive, demonstrating that PRC2 defects play a functional role in conferring sensitivity to MEK/BET inhibitors (Figures 4D and E). Similar to innately sensitive cells, HOXC10 expression was inhibited by BET and MEK/BET inhibitors in these newly sensitized cells (Figure S4B). Most importantly, ectopic HOXC10 expression also rescued this acquired sensitivity (Figure

4F and Figure S4C). These observations demonstrate that PRC2 suppression triggers the aberrant expression of HOXC10 in NSCLC. Consequently, these cells become dependent on HOXC10 expression and are sensitized to BET/MEK inhibitors.

Heterozygous defects in the PRC2 components are common in *KRAS*-mutant NSCLC

Approximately 33% of *KRAS*-mutant tumors exhibit heterozygous loss of at least one PRC2 (Figure 4G, TCGA). While the observation that PRC2 defects were largely restricted to heterozygous events was somewhat unexpected, heterozygous mutations are known to be important in myeloid malignancies (Margueron and Reinberg, 2011) and in mouse models of lymphoma (Ntziachristos et al., 2012). Consistent with cell line analysis, *HOXC10* expression inversely correlated with PRC2 activity in human tumors. Specifically, when *KRAS*-mutant tumors were stratified into those with de-repressed PRC2 targets (i.e. high target expression, low PRC2 activity) versus those with repressed PRC2 targets (i.e. low target expression, high PRC2 activity), *HOXC10* was more highly expressed in “PRC2 low” tumors (Figure 4H). Nevertheless, while PRC2 defects account for much of the *HOXC10* expression in $KRAS^{mut}$ NSCLC, the discrepancy between the frequency of HOXC10 overexpression (51%) versus PRC2 heterozygous alterations (33%) suggests that additional unknown mechanisms may also be involved. Therefore, HOXC10 expression itself is likely to be a superior predictive marker of sensitivity to MEK/BET inhibitors.

HOXC10 and MEK cooperatively control the expression of Pre-RC proteins

We next investigated the mechanism by which HOXC10 suppression regulated death. Notably, while WT HOXC10 suppressed cell death triggered by MEK/BET inhibitors, a HOXC10 protein lacking the homeobox domain did not, underscoring the importance of transcription (Figure 5A and Figure S5A). Therefore, we performed gene ontology (GO) enrichment analysis on the transcripts that were significantly suppressed by BET/MEK inhibitors, prior to cell death. Gene sets related to DNA replication initiation, strand elongation, and replication checkpoints were the most significantly enriched (Figure 5B). Importantly, these genes are not universally enriched in tumor cells treated with cytotoxic agents (Malone et al., 2017). Genes associated with DNA replication initiation (the top scoring list), included many essential components of the pre-replication complex (pre-RC): CDC6 and MCM2–7.

We then identified genes suppressed by MEK/BET inhibitors which were re-elevated in the presence of ectopic HOXC10. GO analysis identified the DNA replication initiation gene list as the most highly enriched and significant hit (log2 fold enrichment = 3.73, p value = 1.40E-10, FDR = 7.77E-08; Figure 5C), raising the possibility that the suppression of these genes could be playing a causal role in cell death.

Pre-RC components bind DNA in well-defined steps in G1, and mark all potential replication origins, a subset of which become activated in S phase (Mechali, 2010). If insufficient numbers of origins are present, replication forks can stall, collapse, and trigger DNA damage and cell death (Zeman and Cimprich, 2014). Microarray analysis revealed that combined MEK/BET inhibitors suppressed multiple pre-RC genes (Figure 5D). Q-PCR confirmed that MEK and BET inhibitors each contributed to the suppression, but maximal

inhibition was only observed in the presence of both agents (Figure 5E). The cooperative effects of MEK/BET inhibitors on pre-RC components was confirmed by immunoblots (Figure 5F). CDC6 and MCM2–7 proteins are all obligate components of the pre-RC complex, and therefore loss of any one protein inhibits its function. Therefore, we focused our analysis on CDC6 and MCM5, as they were the most potently suppressed genes in these cells (Figure 5D), although the suppression of MCM6 and 7 are shown in Figure S5B.

MCM5 and CDC6 were not generally suppressed by cytotoxic agents, as gemcitabine and cisplatin had no effect on expression (Figure 5G). Moreover, ectopic HOXC10 expression substantially rescued the expression of all of the suppressed pre-RC genes, albeit not completely, due to the contribution of MEK inhibitors (Figure 5H). The restoration of MCM5 and CDC6 protein levels by ectopic HOXC10 was confirmed by immunoblots (Figure 5I). Together these results demonstrate that HOXC10 and MEK both cooperatively regulate the expression of pre-RC genes in sensitive NSCLC cells.

MCM5 and *CDC6* genes are induced in G1 and mRNA levels peak at the G1/S boundary (Ohtani et al., 1998). To exclude the possibility that the suppression of these genes was due to changes in cell cycle distribution, a cell cycle sorting experiment was performed. Importantly, MCM5 and CDC6 expression were suppressed both in sensitive cells that were either in the G1 or the S phases of the cell cycle, in response to BET/MEK inhibitors (Figure 5J), suggesting that these changes were not a secondary consequence of effects on the cell cycle.

The suppression of pre-RC components plays an active role in promoting cell death

Finally, to determine whether the suppression of pre-RC proteins was playing a causal role in triggering death, MCM5 or CDC6 expression were reduced by siRNA sequences. In two sensitive cell lines, further suppression of either CDC6 or MCM5 by RNAi potentiated the cytotoxic response of the combination (Figure 5K, left, Figure S5C). By contrast, knockdown of MCM5 or CDC6 in resistant cells did not enhance the effects of BET/MEK inhibitors and responses remained cytostatic (Figure 5K right, Figure S5C). These observations suggest that HOXC10-expressing cells are more sensitive to reduced levels of origin proteins, which are coordinately regulated by HOXC10 and the Ras/MEK pathways, and that the suppression of these pre-RC proteins plays an active role in triggering cell death. The differences between sensitive and resistant cells will be discussed below.

MEK and HOXC10 coordinately regulate pre-RC proteins via E2F

We next investigated the mechanism by which the Ras/MEK and HOXC10 pathways cooperatively regulate pre-RC proteins. Notably, MCM genes and *CDC6* are well-established E2F targets. As such, E2F levels dictate not only whether a cell can enter S phase, but are also required to produce the machinery necessary for replication (Ren et al., 2002). Given the known role of many HOX genes in instructing proliferation versus arrest during development, we investigated whether HOXC10 might cooperatively regulate E2F expression levels, along with the Ras/ERK pathway in these cells.

MEK inhibitors suppress E2F in part by suppressing cyclin D1. Accordingly, MEK inhibitors suppressed E2F1 by > 2-fold (Figure 6A). BET inhibitors also suppressed E2F1

expression 1.5-fold and together both agents suppressed levels 4.2-fold (Figure 6A). E2F1 suppression was confirmed by Q-PCR and the cooperative effect of these agents was evident by ssGSEA analysis of E2F1 targets (Figure S6A, Figure 6B). The cooperative suppression of canonical E2F1 target genes (*MCM5* and *CDC6*) was confirmed by Q-PCR and immunoblots (Figures 5E, F and Figure S5B). Importantly, HOXC10 reconstitution restored ≥ half of the E2F1 expression in cells treated with MEK/BET inhibitors, bringing E2F1 levels back to those observed in response to MEKi alone (Figure 6C), demonstrating that HOXC10 regulates E2F1 transcription. These findings mirrored the partial rescue of CDC6 and MCM5 expression conferred by HOXC10 reconstitution (Figure 5H, I). These data demonstrate that HOXC10 and MEK cooperatively regulate the expression of E2F1 and accordingly key E2F1 target genes (e.g. *CDC6* and *MCM5*).

A cartoon depicting our model is shown in Figure 6D. The data discussed thus far demonstrate that MEK inhibitors and BET inhibitors (the latter through HOXC10) coordinately suppress E2F1 and pre-RC gene expression in NSCLCs. However, if HOXC10 truly functions by regulating E2F1 expression, then the rescue of cell death conferred by ectopic HOXC10 should be prevented by a genetic reduction of E2F1 levels. RNAi-mediated reduction of E2F1 levels alone was not sufficient to arrest these cells and had no effect on the potent cytotoxic effects of MEK/BET inhibitors (Figure 6E). As shown, ectopic expression of HOXC10 substantially attenuated the cytotoxic effects of MEK/BET inhibitors; however, E2F1 suppression reversed these effects and restored sensitivity to these agents (Figure 6E, Figure S6B). These studies demonstrate that HOXC10 mediates its effects in this therapeutic context, by critically regulating E2F1 expression.

BET/MEK inhibitors kill HOXC10 expressing NSCLC by inducing replication fork stalling and DNA damage

Acute suppression of pre-RC proteins would only be expected to trigger cell death in cycling cells. Interestingly, in some cell types suppression of MCM5 or CDC6 cause a growth arrest and no cell death, due to a licensing checkpoint at the G1/S boundary (Blow and Gillespie, 2008). However, in some cancer cells MCM5 or CDC6 suppression does not cause a growth arrest. Instead, these cells die in the presence of agents that further enhance replication stress (Feng et al., 2003; Lau et al., 2006; Shreeram et al., 2002). In this setting death occurs because cells do not completely arrest in G1 and therefore proceed to S phase with too few origins of replication, resulting in replication fork collapse and DNA damage (Lau et al., 2009). We examined the effects of MEK/BET inhibitors on cell cycle dynamics. Interestingly, these agents induced a potent G1 cell cycle arrest in resistant cells within 24 hours (Figure 7A), consistent with suppression of proliferation and absence of cell death observed in Figure 1D. By contrast, sensitive cells did not completely arrest in G1 and 27–41% of the cells were still detected in S and G2/M (Figure 7B). This observation suggests that sensitive cells are cycling as death is occurring.

Based on the paradigm described above, if these agents were triggering cell death by suppressing origins of replication, we would expect to see 1) a depletion of pre-RC components bound to DNA and 2) replication fork stalling in S phase and ultimately DNA damage. In Figure 5J, we demonstrated that obligate pre-RC genes were potently

suppressed by MEK/BET inhibitors in both G1 and S phases. Chromatin fractionation further confirmed that this suppression resulted in a dramatic loss of DNA-bound CDC6, MCM5 and MCM6 (Figure 7C). Moreover, DNA fiber analysis demonstrated that these agents caused profound replication fork stalling in sensitive cell lines (Figure 7D, E and Figure S7A,B). While eukaryotic cells have a reserve of replication origins, a substantial reduction of replication origins is sufficient to cause DNA damage in cells that continue to cycle through S phase (Ge et al., 2007; Ibarra et al., 2008). Accordingly, MEK/BET inhibitors potently induced DNA damage in sensitive but not resistant cell lines (Figure 7F). Kinetic studies demonstrated that CDC6 was potently suppressed within 8 hours, while MCM5 levels decreased more gradually over 24 hours (Figure 7G). Accordingly, phospho-γ-H2AX was elevated at 12 hours, following the loss of CDC6, and became maximal at 24 hours (Figure 7G) whereas apoptosis was triggered between 12–24 hours depending on the cell line (Figure 1D). These findings demonstrate that lung cancers with PRC2/HOXC10 defects do not arrest in response to BET/MEK inhibitors, but instead continue to cycle. Nevertheless, these cells are dependent on HOXC10 for producing sufficient levels of pre-RC proteins. As such, the suppression of pre-RC proteins plays an active role in triggering cell death by causing fork stalling and DNA damage, revealing a unique link between epigenetic defects, homeobox genes, and replication.

DISCUSSION

Here we describe a promising therapeutic combination for *KRAS*-mutant NSCLCs. Specifically, combined MEK/BET inhibitors are effective in approximately 50% of human NSCLCs and trigger potent tumor regression in xenograft and PDX models *in vivo*. While the recent development of KRAS inhibitors represents an important advance, the data presented here raise the intriguing possibility that, similar to MEK inhibitors, the effects of these agents might be further enhanced by the addition of BET inhibitors. Furthermore, in contrast to $KRAS^{G12C}$ inhibitors, this combination is effective in all *KRAS*-mutant subtypes highlighting the broad potential applicability of this approach. Regardless, these data provide strong scientific rationale for evaluating the combined effects of BET and MEK inhibitors, and possibly other Ras pathway inhibitors, in *KRAS*-mutant NSCLC.

We also identified a distinct yet common subset of *KRAS*-mutant lung cancers. Specifically, sensitive tumors universally express high levels of the homeobox gene, HOXC10. HOX genes are developmental regulators that are overexpressed in a variety of cancers. Accordingly, many HOX genes upregulated in cancers are normally expressed in the corresponding tissue during development (Abate-Shen, 2002). However, HOX genes not normally expressed in a tissue can also be “newly” expressed in tumors. In NSCLC, HOXC10 appears to fall into the latter category, as there is no current evidence that HOXC10 is expressed during lung development. Regardless, we show that HOXC10 is a biomarker that predicts sensitivity to combined BET/MEK inhibitors, and that its suppression plays a critical role in mediating the therapeutic response.

Notably, HOXC10 is frequently, but not exclusively, deregulated in NSCLC as a consequence of defects in PRC2 genes. Heterozygous loss of PRC2 components is common in NSCLC, while homozygous loss is rare. This observation is consistent with accumulating

evidence that partial defects in PRC2 activity appear to play a role in the development of other tumor types (Margueron and Reinberg, 2011), and suggest that there may be a selection for maintaining one intact allele in lung cancer, possibly due to effects on the *CDKN2A* locus or other tumor suppressor genes (Bracken et al., 2007). Regardless, the data presented here illustrate how specific epigenetic defects can confer therapeutic vulnerabilities and support the broader approach of developing therapies that co-target oncogenic and epigenetic proteins.

These studies further show that HOXC10 functions by regulating E2F and pre-RC genes in NSCLC. This observation makes teleological sense in that HOX genes are typically involved in maintaining an undifferentiated, proliferative state during development and are downregulated as cells differentiate. Therefore, HOX genes might be expected to send signals that directly permit and/or instruct proliferation. In the context of NSCLCs, defects in the PRC2/HOXC10 axis appear to override cues to stop proliferating. Indeed, resistant cells that lack these defects, arrest in G1 in response to MEK/BET inhibitors. By contrast, those that harbor PRC2 alterations and express HOXC10 are able to proceed through to S phase. However, because HOXC10 and pre-RC genes are suppressed by these agents, replication forks stall, ultimately triggering DNA damage and cell death. These observations reveal a unique cooperative role for HOXC10, together with the Ras pathway, in regulating E2F and replication proteins in NSCLC.

Finally, it should be emphasized that biomarkers are critical for patient selection and ultimately dictate the success of clinical trials. The clinical development of BET inhibitors has been challenging because in most settings biomarkers that predict efficacy have not been identified. In this study we identified a functional, predictive biomarker for this BET inhibitor-based combination in NSCLC. HOXC10 can be readily detected by immunohistochemistry, thus providing a promising and clinically tractable biomarker that can be used to select patients. The observation that HOXC10 suppression is essential for cell death suggests that it may also be useful in post-treatment biopsies to assess target inhibition. Thus altogether, these studies have identified a promising therapeutic strategy for *KRAS*-mutant NSCLCs with a clinical path for translation and have also provided important insight into lung cancer by mechanistically linking epigenetic defects, homeobox genes, and replication.

STAR METHODS

LEAD CONTACT AND MATERIAL SHARING

Further information and requests for resources and reagents should be directed to and will be fulfilled by the Lead Contact, Karen Cichowski (kcichowski@rics.bwh.harvard.edu). This study did not generate new unique reagents.

EXPERIMENTAL MODEL AND SUBJECT DETAILS

Human material—We obtained snap-frozen and unstained immunohistochemistry slides of human lung tumor samples from patients with *KRAS*-mutant lung adenocarcinoma from the archives and biobank of the Belfer Institute for Applied Cancer Science at the

Dana-Farber Cancer Institute. All patients provided written informed consent for the use of the specimen and the studies were performed in accordance with the Declaration of Helsinki, and approved by the Dana-Farber Cancer Institute Institutional Review Board. Three of these tumors were obtained as snap frozen samples, crushed, and dissolved into 1% SDS boiling lysis buffer. The HOXC10 protein levels of these tumor samples were assayed by western blot and levels were compared to high- and low-expressing HOXC10 human lung cancer cell lines. A HOXC10-high tumor was selected for further study in a PDX *in vivo* mouse model. These same tumors were also obtained as slides and used for immunohistochemistry staining of HOXC10.

Cell lines

Human lung cancer cell lines were purchased from the ATCC. All cells were cultured in RPMI media supplemented with 10% FBS and 1% streptomycin/penicillin at 37°C under 5% CO2 with the exception of NCI-H23, NCI-H1435, NCI-H1792, SKLU-1 which were all cultured in DMEM media supplemented similarly and at same temperature and growth conditions. The RRIDs of each cell line is listed in the Key Resources Table. The genomic identity of each cell line was not authenticated. Cell lines were tested to confirm lack of mycoplasma contamination. The sex of each lung cancer cell line is as follows, male sex: A549, NCI-H2444, NCI-H1355, NCI-H1373, NCI-H1792, NCI-H2030, NCI-H23, NCI-H441, and NCI-H460 and female sex: HCC44, NCI-H1435, NCI-H1573, NCI-H1838, NCI-H1944, and SK-LU-1.

Animals

Human Lung Cancer Cell Line-Derived Xenograft models: Animal procedures were approved by the Center for Animal and Comparative Medicine at Harvard Medical School in accordance with the NIH Guide for the Care and Use of Laboratory Animals and the Animal Welfare Act. Cancer cell line-derived xenograft experiments were performed in 6–8 week old female Nu/Nu mice purchased from Charles River laboratories (RRID: IMSR_CRL:088). The same procedure outlined below was used for each cell line derived xenograft experiment including NCI-H1573, NCI-H23, and A549 cell lines. Cells were tested for mycoplasma before injection into flank of mice. More information about the generation of these models is listed below in method details.

Human Lung Cancer Tumor-Derived PDX model: A HOXC10-high tumor was identified from the patient tumors obtained from the Belfer Institute, and this tumor was used to create a lung cancer PDX model. The creation and animal care of the mouse model including subsequent treatments and measurements were performed by the Experimental Therapeutics (ETx) Core at the Dana-Farber Cancer Institute. Briefly, the selected patient tumor was expanded in 6–8 week old female NOD-SCID mice and these expanded tumors were then harvested and re-implanted into mice that were then used for efficacy study. More information about the generation and treatment of this model is listed below in method details.

METHOD DETAILS

Infections and Transfections—shRNA or cDNA constructs were prepared and virus was harvested as previously described (McLaughlin et al., 2013). Virus was incubated with target cells for 6 to 16 hours at a 1:2–1:10 dilution with 8-μg/mL polybrene. For LACZ and HOXC10-infected cells, infection was performed twice, first for 16 hours overnight at 1:2 dilution, then for 6 hours the following day with a fresh 1:2 virus dilution, and cells were allowed to recover for 24 hours before selection. Infected cells were selected in 0.5 to 2.0 μg/mL puromycin or 1 to 2 μg/mL blasticidin, depending on the construct and optimized for each cell line. Selection continued until uninfected control cells were dead, approximately 3–5 days depending on the cell line. For experiments with two constructs, infections were performed sequentially. The first construct was infected and selected followed by second construct infection and selection. Constructs using different selection markers were used so that all cells were doubly selected by both puromycin and blasticidin. For transfections, cells were transfected for 16 hours with 10 μmol/L siRNA constructs using a 1:400 dilution of Lipofectamine RNAiMAX (Invitrogen, cat. # 13778–075) in antibiotic-free media.

Drug concentrations—For all *in vitro* experiments throughout this manuscript the following drug concentrations were used: MEKi (PD901/PD-325901=500 nM); BETi (JQ1=1000 nM), BETi (AZD5153=500 nM); MEKi (trametinib=10 nM), with the exception of the pilot experiment in Figure 1A where PD901 was used at 1000 nM. However, the same sensitive cell lines from that experiment (H1573, H23) are also shown in Figure 1B using 500 nM PD901. Gemcitabine and cisplatin were used at 500 nM and 10 μM, respectively. If not otherwise specified, PD901 and JQ1 were used in each figure.

Short-term Cellular Proliferation Assays—75,000–100,000 cells per well were seeded onto 6-well plates in appropriate media. 24 hours later cells were counted for day 0 timepoints. Drug treatments commenced on day 0. Media was not replaced over the course of 72 hours and day 3 counts were completed in triplicate on day 3 to determine the change in cell number compared to day 0. Proliferation experiments that included siRNA knockdown were performed on cells approximately 24 hours after the initial transfection.

Incucyte Cell Proliferation and Death Assays—Cells were infected with IncuCyte Nuclight red (mKate2) reagent (#4625) and selected in puromycin to create stable cell lines. Nuclight versions of each cell line were plated at 3000–4000 cells/well in a 96 well plate. Approximately 24 hours later, the media was removed and media containing 1:1000 green caspase 3/7 apoptosis assay reagent (#4440) and appropriate drug concentrations was added. The 96 well plate was then placed in the Incucyte instrument and images were taken every two hours over the course of five days. The Incucyte software was then trained to count the cells based on the number of red-expressing nuclei in the field of view. Four images were taken per well and averaged and triplicate wells were counted per condition. Cell death is assayed by the presence of yellow cells which contain green signal (caspase reagent) overlapping with red signal (nuclei). Cell number is assayed as the number of red nuclei minus the number of dead (yellow) overlapping nuclei. Cell number and caspase counts are calculated for every Incucyte reading and normalized to Day 0 to create data graphs.

Long-term Colony growth Assays—Cells were seeded at 5000 (H1355, H23, H1573, H1944) or 2000 (HCC44) cells per well in 12-well plates and treated with DMSO, 500nM MEKi (PD901), 1000nM BETi (JQ1) or the MEKi/BETi combination for 1–3 weeks. Afterwards, cells were fixed, stained and photographed.

IC50 Analysis—Cells were plated in 96-well plates and 3 technical replicates were performed for each condition. At 24 hr one plate of cells was frozen (−80°C) representing the day 0 plate. At this time, 9-point serial dilutions of the drugs of interest ranging from 20μM to 5nM were added to the remaining plates. After 72 hr, each of the plates was frozen. After freezing, the plates (day 0 and 3) were thawed simultaneously and cells were quantified using CellTiter-Glo (Promega) as per the manufacturer's instructions. The raw CellTiter-Glo assay readout values were considered proportional to the number of viable cells and used as surrogates for cell count values. Relative cell growth was calculated (day 3 versus day 0) and normalized to 3 population doublings. Dose response curves were subsequently fitted across all tested concentrations and IC50 values were derived using GraphPad Prism 8.

Xenografts and *in vivo* drug studies—Briefly, 2.5×10^6 cells in 50% matrigel/media were injected into the flank of each mouse. Ten tumors were used per treatment arm. Treatment commenced at day 0 when tumors reached an average size of 300–500mm^3 approximately 3–4 weeks after initial injection. Same procedure was followed with the xenografts of NCI-H23, NCI-H1573 and A549.

For all mouse experiments, including two human xenografts and one patient-derived xenograft, PD-0325901 was administered at 1.5 mg/kg daily by oral gavage (vehicle: 0.5% (w/v) methylcellulose solution with 0.2% (v/v) polysorbate 80 (Tween 80)). JQ1 was administered at 45 mg/kg intraperitoneally daily in a 10% (2-hydroxypropyl)-β-cyclodextrin solution (C0926, Sigma). AZD5153 was administered at 2.5mg/kg by oral gavage daily (vehicle: 0.5% hydroxymethylcellulose, 0.1% Tween80). Trametinib was administered at 0.6 mg/kg by oral gavage daily (vehicle: 0.5% hydroxymethylcellulose, 0.1% Tween80, pH=8). Compounds given in combination were administered sequentially. Mice were started on treatment when tumor size reached 300–500 mm^3 and were randomly assigned to experimental groups. Tumor size was measured every 2–3 days by calipers. Tumor volume was calculated using the standard formula L x W^2 × 0.52.

Patient Derived Xenograft Model—In collaboration with the Belfer Institute and the BWH Experimental Therapeutics Core, we obtained three PDX tumor samples from patients with *KRAS*-mutant lung adenocarcinoma. These tumors were crushed and dissolved into 1% SDS boiling lysis buffer. HOXC10 protein levels were assayed by western blot and levels were compared to high and low expressing HOXC10 human lung cancer cell lines. A HOXC10-high PDX was selected for further study. This PDX tumor was expanded in NOD-SCID mice and these expanded tumors were then harvested and re-implanted into experimental mice. Ten tumors were enrolled per treatment arm when volume reached approximately 150–200 mm^3. Mice were sacrificed when tumor volumes reached >2000 mm^3. All dosing was done as described above. The Experimental Therapeutics Core conducted all animal care and tumor measurements.

Differential mutational analysis, copy number analysis, and two class comparison of expression data—Public expression, mutational, and copy number data was also downloaded from the Broad Institute Cancer Cell Line Encyclopedia via the UCSC cancer genome browser. Mutational and copy number data was assayed on the cBioPortal visualizer (http://www.cbioportal.org/). To compare the gene expression profiles of sensitive and resistant cell lines, expression data (RNAseq) was downloaded from the Broad Institute CCLE database. Data from the ten cell lines was isolated and organized into two groups, either sensitive or resistant, as defined in Figure 1B. The expression data of each group was compared in aggregate using the BRBArrayTools Version 4.5.1 plug-in in Microsoft Excel 2016 to identify differentially expressed single genes. A two-class comparison analysis (F-test on ratios of geometric means of individual genes between classes) was performed at a corrected p value of 0.001 to obtain the differentially expressed genes shown in Figure 2A.

Analysis of HOXC10 expression and PRC2 signatures—Public expression, mutational, and copy number data was downloaded from the TCGA-LUAD project. Expression of HOXC10 in normal tissue was assayed for mean and standard deviation. Tumor samples were then stratified according to HOXC10 expression levels relative to the normal tissue. Overexpression was defined as two standard deviations over the mean expression in normal tissue. Matched *KRAS*-mutant tumor-normal samples were also identified. Expression data of high-HOXC10 and low-HOXC10 tumors was also obtained from the TCGA and single sample gene set enrichment analysis (ssGSEA) was performed on the data to determine the relative level of PRC2 target expression in each group of tumors. Similarly, the same ssGSEA analysis was performed on all normal and tumor samples. Samples were then stratified according to high and low PRC2 target expression (>1 SD over normal tissue) and then corresponding HOXC10 expression was assayed.

Microarray RNA expression analysis—RNA was isolated from NCI-H1573 (or LACZ and HOXC10-expresssing NCI-H1573) cells 24 hours after treatment with indicated drugs. RNA was isolated using TRIzol, following the manufacturer's protocol and RNA cleanup was performed using the Qiagen RNeasy kit (#74104). The Molecular Biology Core Facilities at Dana-Farber Cancer Institute hybridized RNA to the Affymetrix Human 2.0 STS array chip. To determine genes and genesets that were differentially expressed among treatment groups a two-class comparison analysis (F-test on ratios of geometric means of individual genes between classes) was performed using BRB-Array tools to identify differentially expressed single genes and the Broad Institute's GSEA tool to identify differentially expressed genesets. Geneset Enrichment analysis (GSEA) was performed on both publicly available data as well as microarray data. Genelists such as "Ras transcriptional output" and "compiled PRC2 targets" are lists compiled from publicly available GSEA lists (MSigDB) from the C6 collection (oncogenic signatures) of the Broad Institute. "Ras transcriptional output" is the union of significantly downregulated genes from seven mutant RAS gene lists from C6. "compiled PRC2 targets" is the union of significantly downregulated genes from three PRC2 genelists from C6. Genelists can be found in supplementary materials.

Quantitative PCR—RNA was harvested from cells after indicated treatments using Trizol (Invitrogen) and was extracted by phenol-chloroform extraction. Primers for *MCM5* were (5′–3′):

AGCATTCGTAGCCTGAAGTCG (forward) and CGGCACTGGATAGAGATGCG (reverse).

Primers for *CDC6* were (5′–3′): GACCTCAAGAAGGAACTG (forward) and ATACCTCTTCCTGACAAATCTC (reverse). Primers for *HOXC10* were (5′–3′): CTATCCGTCCTACCTCTCGCA (forward) and ACATGCAGCAGACATTCTCCT (reverse).

Primers for *E2F1* were (5′–3′): AGATGGTTATGGTGATCAAAGCC (forward) and ATCTGAAAGTTCTCCGAAGAGTCC (reverse). All samples were normalized to human *GAPDH or UBC*. Primers for *GAPDH* were (5′–3′) GCCGGCTCCGTTATGG (forward) and AACCTGGTTCATCATCACTA (reverse). Primers for *UBC* were (5′–3′) GCCGGCTCCGTTATGG (forward) and AACCTGGTTCATCATCACTA (reverse).

Flow Cytometry

Cell cycle fractionation: Cells were seeded onto 15-cm plates overnight. The next morning, plates were treated with either DMSO or combined treatment. Following 24 hours of treatment, cells were trypsinized and resuspended at a concentration of $<1\times10^6$ cells/mL in complete media containing 10ug/mL of Hoechst stain (BDBiosciences #33342). Cells were incubated for 1 hour at 37°C and then pelleted and re-suspended in 1X PBS prior to sorting. Each treatment group was analyzed on a BDAria Sorter. Cell populations were fractionated into G1, S, and G2/M populations based on Hoechst staining. At least 100,000 cells were collected per cell cycle fraction. RNA was extracted from resulting fractions using an RNeasy kit from Qiagen. qPCR analysis was performed on isolated RNA according to protocol defined above.

Cell cycle analysis: Cells were plated to 60–70% confluence on 10-cm plates. The next day, media was changed with appropriate concentration of drug and cells were incubated for 16 or 24 hours. After drug treatment, cells were trypsinized, resuspended, and washed in 1X PBS. Cells were then suspended in propidium iodide staining media, incubated for thirty minutes at room temperature, then analyzed on a DPX11 analyzer. FlowJo software was used for cell cycle analysis and figure creation.

DNA Fiber Analysis—Cells were plated at 50% confluence onto 15-cm plates. Media was changed the next day and new media with appropriate drug concentrations was added. NCI-H1573 and H23 cells were treated with vehicle control or drug combo for fourteen hours and then the thymidine analog CldU was spiked into media for incorporation into DNA. After two hours, CldU was washed out and another thymidine analog, IdU, was added. DNA fiber spreading and staining were performed after which CIdU and ldU were detected using red and green-fluorescent secondary antibodies respectively via confocal microscopy. The ratios of green vs. red fiber track lengths (IdU/CIdU) were quantified using ImageJ to determine the presence of slowing and/or stalled replication forks in each

condition. The high outliers (IdU/CIdU ratios) were removed for graphing purposes, but with or without these outliers the difference between vehicle and combo treated cells were statistically significant ($p<0.0001$, 2-tailed t-test).

Chromatin Isolation experiment—To determine the chromatin-bound fraction of CDC6 and MCM5 in response to treatment, a chromatin isolation experiment was performed on sensitive cell lines based on a protocol from (Wysocka et al., 2001). Briefly, following 24 hours of treatment with DMSO, 500 nM MEKi (PD901), 1000 nM BETi (JQ1) or the MEKi/BETi combination, $1 \times 10^7 – 2 \times 10^7$ were harvested by cell scraper and spun down at 1000 rpm for 2 minutes. Cell pellet was washed twice with PBS and then resuspended in buffer A (containing 10mM HEPES, 10mM KCl, 1.5mM $MgCl_2$, 0.34M Sucrose, 10% Glycerol, 1mM DTT, and protease inhibitor cocktail). Following resuspension, Triton X-100 was added to a final concentration of 0.1% and cells were incubated on ice for 8 minutes. Cells were spun down and supernatant was separated from pellet (nuclei). Pellet was washed again with Buffer A and then lysed for 30 minutes at room temperature with Buffer B (containing 3mM EDTA, 0.2mM EGTA, 1mM DTT, and protease inhibitor cocktail). Following lysis, pellet was spun down again. This pellet (which now is enriched for chromatin) was washed again with Buffer B. Following wash, pellet was resuspended in SDS sample buffer, boiled, and then analyzed by western blot for CDC6 and MCM5 in the presence or absence of drug treatment. This chromatin-enriched fraction was compared to whole cell lysate by western blot.

Quantification and statistical analysis—For quantitative measurements, graphs represent mean ± SD. Where indicated data are presented as $\log_2$ fold change over initial measurements. Changes in tumor volume are presented in a waterfall plot with each bar representing the change in tumor volume of an individual animal in the study. A bar over the zero line indicates tumor growth and a bar under the zero line indicates tumor shrinkage. 2-tailed unpaired t tests, and Mann-Whitney U tests was used to compare data sets where indicated, and p values are shown. Effects of cell line and drug treatment on cell proliferation were analyzed by two-way Anova. Once significant effects of cell line and treatment were found, multiple comparisons were tested for significance using Tukey's post-hoc test. A p value less than or equal to 0.05 was considered significant. Data were graphed and analyzed using GraphPad Prism v.6 with the exception of microarray data which was analyzed and visualized using BRB-Array tools. Cell viability assays are representative ≥ 3 biological replicates.

DATA AND CODE AVAILABILITY

The microarray expression datasets generated during this study are available at Gene Expression Omnibus SuperSeries # GSE118909.

Supplementary Material

Refer to Web version on PubMed Central for supplementary material.

ACKNOWLEDGEMENTS

This work was supported by the NCI (R01CA111754) and the Ludwig Center at HMS.

DECLARATION OF INTERESTS

PAJ consults for AstraZeneca, Boehringer Ingelheim, Eli Lilly and Company, and Mirati Therapeutics; has sponsored research agreements with AstraZeneca, Boehringer Ingelheim, Eli Lilly and Company, Astellas Pharmaceuticals and Revolution Medicines. S.J.E. is a founder of TSCAN Therapeutics, MAZE Therapeutics and Mirimus and is on the SAB of CRISPR Therapeutics, Homology Medicine, TSCAN Therapeutics, XChem, and advises for MPM.

REFERENCES

Abate-Shen C. (2002). Deregulated homeobox gene expression in cancer: cause or consequence? Nat Rev Cancer 2, 777–785. [PubMed: 12360280]

Amorim S, Stathis A, Gleeson M, Iyengar S, Magarotto V, Leleu X, Morschhauser F, Karlin L, Broussais F, Rezai K, et al. (2016). Bromodomain inhibitor OTX015 in patients with lymphoma or multiple myeloma: a dose-escalation, open-label, pharmacokinetic, phase 1 study. Lancet Haematol 3, e196–204. [PubMed: 27063978]

Berthon C, Raffoux E, Thomas X, Vey N, Gomez-Roca C, Yee K, Taussig DC, Rezai K, Roumier C, Herait P, et al. (2016). Bromodomain inhibitor OTX015 in patients with acute leukaemia: a dose-escalation, phase 1 study. Lancet Haematol 3, e186–195. [PubMed: 27063977]

Blow JJ, and Gillespie PJ (2008). Replication licensing and cancer--a fatal entanglement? Nat Rev Cancer 8, 799–806. [PubMed: 18756287]

Bracken AP, Kleine-Kohlbrecher D, Dietrich N, Pasini D, Gargiulo G, Beekman C, Theilgaard-Monch K, Minucci S, Porse BT, Marine JC, et al. (2007). The Polycomb group proteins bind throughout the INK4A-ARF locus and are disassociated in senescent cells. Genes Dev 21, 525–530. [PubMed: 17344414]

Cancer Genome Atlas Research, N. (2014). Comprehensive molecular profiling of lung adenocarcinoma. Nature 511, 543–550. [PubMed: 25079552]

De Raedt T, Beert E, Pasmant E, Luscan A, Brems H, Ortonne N, Helin K, Hornick JL, Mautner V, Kehrer-Sawatzki H, et al. (2014). PRC2 loss amplifies Ras-driven transcription and confers sensitivity to BRD4-based therapies. Nature 514, 247–251. [PubMed: 25119042]

Delmore JE, Issa GC, Lemieux ME, Rahl PB, Shi J, Jacobs HM, Kastritis E, Gilpatrick T, Paranal RM, Qi J, et al. (2011). BET bromodomain inhibition as a therapeutic strategy to target c-Myc. Cell 146, 904–917. [PubMed: 21889194]

Feng D, Tu Z, Wu W, and Liang C. (2003). Inhibiting the expression of DNA replication-initiation proteins induces apoptosis in human cancer cells. Cancer Res 63, 7356–7364. [PubMed: 14612534]

Feng X, Li T, Liu Z, Shi Y, and Peng Y. (2015). HOXC10 up-regulation contributes to human thyroid cancer and indicates poor survival outcome. Mol Biosyst 11, 2946–2954. [PubMed: 26279264]

Flaherty KT, Infante JR, Daud A, Gonzalez R, Kefford RF, Sosman J, Hamid O, Schuchter L, Cebon J, Ibrahim N, et al. (2012). Combined BRAF and MEK inhibition in melanoma with BRAF V600 mutations. N Engl J Med 367, 1694–1703. [PubMed: 23020132]

Ge XQ, Jackson DA, and Blow JJ (2007). Dormant origins licensed by excess Mcm2–7 are required for human cells to survive replicative stress. Genes Dev 21, 3331–3341. [PubMed: 18079179]

Ibarra A, Schwob E, and Mendez J. (2008). Excess MCM proteins protect human cells from replicative stress by licensing backup origins of replication. Proc Natl Acad Sci U S A 105, 8956–8961. [PubMed: 18579778]

Janes MR, Zhang J, Li LS, Hansen R, Peters U, Guo X, Chen Y, Babbar A, Firdaus SJ, Darjania L, et al. (2018). Targeting KRAS Mutant Cancers with a Covalent G12C-Specific Inhibitor. Cell 172, 578–589 e517. [PubMed: 29373830]

Janne PA, van den Heuvel MM, Barlesi F, Cobo M, Mazieres J, Crino L, Orlov S, Blackhall F, Wolf J, Garrido P, et al. (2017). Selumetinib Plus Docetaxel Compared With Docetaxel Alone

and Progression-Free Survival in Patients With KRAS-Mutant Advanced Non-Small Cell Lung Cancer: The SELECT-1 Randomized Clinical Trial. JAMA 317, 1844–1853. [PubMed: 28492898]

Krivtsov AV, and Armstrong SA (2007). MLL translocations, histone modifications and leukaemia stem-cell development. Nat Rev Cancer 7, 823–833. [PubMed: 17957188]

Lau E, Chiang GG, Abraham RT, and Jiang W. (2009). Divergent S phase checkpoint activation arising from prereplicative complex deficiency controls cell survival. Mol Biol Cell 20, 3953–3964. [PubMed: 19587119]

Lau E, Zhu C, Abraham RT, and Jiang W. (2006). The functional role of Cdc6 in S-G2/M in mammalian cells. EMBO Rep 7, 425–430. [PubMed: 16439999]

Lee W, Teckie S, Wiesner T, Ran L, Prieto Granada CN, Lin M, Zhu S, Cao Z, Liang Y, Sboner A, et al. (2014). PRC2 is recurrently inactivated through EED or SUZ12 loss in malignant peripheral nerve sheath tumors. Nat Genet 46, 1227–1232. [PubMed: 25240281]

Lewin J, Soria JC, Stathis A, Delord JP, Peters S, Awada A, Aftimos PG, Bekradda M, Rezai K, Zeng Z, et al. (2018). Phase Ib Trial With Birabresib, a Small-Molecule Inhibitor of Bromodomain and Extraterminal Proteins, in Patients With Selected Advanced Solid Tumors. J Clin Oncol 36, 3007–3014. [PubMed: 29733771]

Lito P, Solomon M, Li LS, Hansen R, and Rosen N. (2016). Allele-specific inhibitors inactivate mutant KRAS G12C by a trapping mechanism. Science 351, 604–608. [PubMed: 26841430]

Maertens O, Kuzmickas R, Manchester HE, Emerson CE, Gavin AG, Guild CJ, Wong TC, De Raedt T, Bowman-Colin C, Hatchi E, et al. (2019). MAPK Pathway Suppression Unmasks Latent DNA Repair Defects and Confers a Chemical Synthetic Vulnerability in BRAF-, NRAS-, and NF1-Mutant Melanomas. Cancer Discov 9, 526–545. [PubMed: 30709805]

Mallo M, and Alonso CR (2013). The regulation of Hox gene expression during animal development. Development 140, 3951–3963. [PubMed: 24046316]

Malone CF, Emerson C, Ingraham R, Barbosa W, Guerra S, Yoon H, Liu LL, Michor F, Haigis M, Macleod KF, et al. (2017). mTOR and HDAC Inhibitors Converge on the TXNIP/Thioredoxin Pathway to Cause Catastrophic Oxidative Stress and Regression of RAS-Driven Tumors. Cancer Discov 7, 1450–1463. [PubMed: 28963352]

Margueron R, and Reinberg D. (2011). The Polycomb complex PRC2 and its mark in life. Nature 469, 343–349. [PubMed: 21248841]

McLaughlin SK, Olsen SN, Dake B, De Raedt T, Lim E, Bronson RT, Beroukhim R, Polyak K, Brown M, Kuperwasser C, and Cichowski K. (2013). The RasGAP gene, RASAL2, is a tumor and metastasis suppressor. Cancer Cell 24, 365–378. [PubMed: 24029233]

Mechali M. (2010). Eukaryotic DNA replication origins: many choices for appropriate answers. Nat Rev Mol Cell Biol 11, 728–738. [PubMed: 20861881]

Misale S, Fatherree JP, Cortez E, Li C, Bilton S, Timonina D, Myers DT, Lee D, Gomez-Caraballo M, Greenberg M, et al. (2019). KRAS G12C NSCLC Models Are Sensitive to Direct Targeting of KRAS in Combination with PI3K Inhibition. Clin Cancer Res 25, 796–807. [PubMed: 30327306]

Ntziachristos P, Tsirigos A, Van Vlierberghe P, Nedjic J, Trimarchi T, Flaherty MS, Ferres-Marco D, da Ros V, Tang Z, Siegle J, et al. (2012). Genetic inactivation of the polycomb repressive complex 2 in T cell acute lymphoblastic leukemia. Nat Med 18, 298–301. [PubMed: 22237151]

Ohtani K, Tsujimoto A, Ikeda M, and Nakamura M. (1998). Regulation of cell growth-dependent expression of mammalian CDC6 gene by the cell cycle transcription factor E2F. Oncogene 17, 1777–1785. [PubMed: 9778043]

Ostrem JM, Peters U, Sos ML, Wells JA, and Shokat KM (2013). K-Ras(G12C) inhibitors allosterically control GTP affinity and effector interactions. Nature 503, 548–551. [PubMed: 24256730]

Patricelli MP, Janes MR, Li LS, Hansen R, Peters U, Kessler LV, Chen Y, Kucharski JM, Feng J, Ely T, et al. (2016). Selective Inhibition of Oncogenic KRAS Output with Small Molecules Targeting the Inactive State. Cancer Discov 6, 316–329. [PubMed: 26739882]

Reck M, and Rabe KF (2017). Precision Diagnosis and Treatment for Advanced Non-Small-Cell Lung Cancer. N Engl J Med 377, 849–861. [PubMed: 28854088]

Ren B, Cam H, Takahashi Y, Volkert T, Terragni J, Young RA, and Dynlacht BD (2002). E2F integrates cell cycle progression with DNA repair, replication, and G(2)/M checkpoints. Genes Dev 16, 245–256. [PubMed: 11799067]

Rouillard AD, Gundersen GW, Fernandez NF, Wang Z, Monteiro CD, McDermott MG, and Ma'ayan A. (2016). The harmonizome: a collection of processed datasets gathered to serve and mine knowledge about genes and proteins. Database (Oxford) 2016.

Sadik H, Korangath P, Nguyen NK, Gyorffy B, Kumar R, Hedayati M, Teo WW, Park S, Panday H, Munoz TG, et al. (2016). HOXC10 Expression Supports the Development of Chemotherapy Resistance by Fine Tuning DNA Repair in Breast Cancer Cells. Cancer Res 76, 4443–4456. [PubMed: 27302171]

Schuettengruber B, Bourbon HM, Di Croce L, and Cavalli G. (2017). Genome Regulation by Polycomb and Trithorax: 70 Years and Counting. Cell 171, 34–57. [PubMed: 28938122]

Shah N, and Sukumar S. (2010). The Hox genes and their roles in oncogenesis. Nat Rev Cancer 10, 361–371. [PubMed: 20357775]

Shreeram S, Sparks A, Lane DP, and Blow JJ (2002). Cell type-specific responses of human cells to inhibition of replication licensing. Oncogene 21, 6624–6632. [PubMed: 12242660]

Singh A, Greninger P, Rhodes D, Koopman L, Violette S, Bardeesy N, and Settleman J. (2009). A gene expression signature associated with "K-Ras addiction" reveals regulators of EMT and tumor cell survival. Cancer Cell 15, 489–500. [PubMed: 19477428]

Stathis A, and Bertoni F. (2018). BET Proteins as Targets for Anticancer Treatment. Cancer Discov 8, 24–36. [PubMed: 29263030]

Stathis A, Zucca E, Bekradda M, Gomez-Roca C, Delord JP, de La Motte Rouge T, Uro-Coste E, de Braud F, Pelosi G, and French CA (2016). Clinical Response of Carcinomas Harboring the BRD4-NUT Oncoprotein to the Targeted Bromodomain Inhibitor OTX015/MK-8628. Cancer Discov 6, 492–500. [PubMed: 26976114]

Wysocka J, Reilly PT, and Herr W. (2001). Loss of HCF-1-chromatin association precedes temperature-induced growth arrest of tsBN67 cells. Mol Cell Biol 21, 3820–3829. [PubMed: 11340173]

Zeman MK, and Cimprich KA (2014). Causes and consequences of replication stress. Nat Cell Biol 16, 2–9. [PubMed: 24366029]

Zeng M, Lu J, Li L, Feru F, Quan C, Gero TW, Ficarro SB, Xiong Y, Ambrogio C, Paranal RM, et al. (2017). Potent and Selective Covalent Quinazoline Inhibitors of KRAS G12C. Cell Chem Biol 24, 1005–1016 e1003. [PubMed: 28781124]

Zhang M, Wang Y, Jones S, Sausen M, McMahon K, Sharma R, Wang Q, Belzberg AJ, Chaichana K, Gallia GL, et al. (2014). Somatic mutations of SUZ12 in malignant peripheral nerve sheath tumors. Nat Genet 46, 1170–1172. [PubMed: 25305755]

Significance:

There are currently no effective treatments for *KRAS*-mutant lung cancers. Here we show that combined MEK/BET inhibitors are effective in half of *KRAS*-mutant NSCLCs and cause potent tumor regression in xenograft and PDX models. We also identify the homeobox gene, *HOXC10*, as a predictive and functional biomarker of the therapeutic response and deconstruct the mechanism by which these agents function. Together these studies have identified a distinct, common subset of NSCLCs along with a promising therapeutic strategy. They have also uncovered a mechanistic connection between epigenetic regulators, homeobox proteins, and replication.

HIGHLIGHTS

- Combined MEK/BET inhibitors are effective in *KRAS* mutant NSCLCs
- Sensitivity is dependent on HOXC10, which is overexpressed in 51% of tumors
- Aberrant HOXC10 expression is largely caused by defects in PRC2 genes
- MEK/BET inhibitors co-suppress Ras output and HOXC10 to cause replication defects

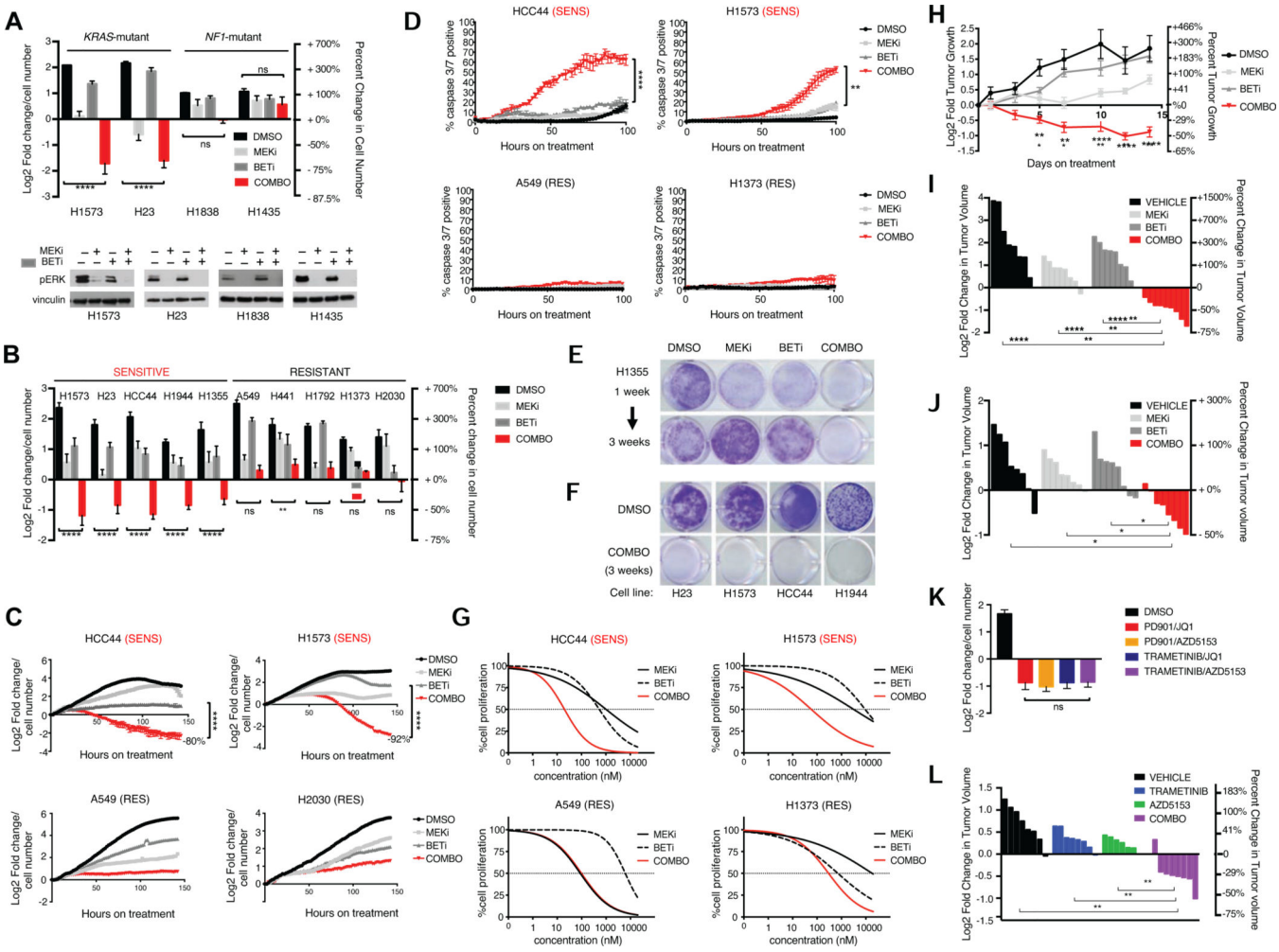

Figure 1. MEK/BET inhibitors trigger death and tumor regression in *KRAS*-mutant NSCLC

(A-B) Mean change in cell number −/+ SD from technical triplicates after 72 hr of treatment as indicated, determined by manual counting. Data representative of ≥ 3 experiments. ****p<0.0001, **p<0.01, Two-way Anova analysis and Tukey's post-hoc test. "ns" = not significant.

(C-D) Live-cell imaging depicting mean cell number (C) or cleaved caspase activity (D) −/+ SD from triplicate wells. ****p<0.0001, **p=0.0022, one-way Anova test and Tukey post hoc.

(E) Colony formation after 1 or 3 weeks.

(F) Colony formation after 3 weeks.

(G) Normalized IC50 curves.

(H) Mean tumor size of H23 xenografts +/− SEM, eight tumors per condition.

(I-J) Waterfall plot depicting size change of H23 (I) and H1573 (J) tumors after 14 days. ****p<0.0001, *p<0.05 (Mann-Whitney test). Each bar depicts one tumor. There were eight tumors per condition.

(K) Mean change in H23 cell number (−/+ SD from technical triplicates) after 72 hr, determined by manual counting (2-tailed t-test).

(L) Waterfall plot depicting the change in size of H1573 tumors after 14 days. **p<0.01 (Mann-Whitney test). Each bar depicts one tumor. There were eight tumors per condition. See also Figures S1 and S2 and Tables S1 and S2.

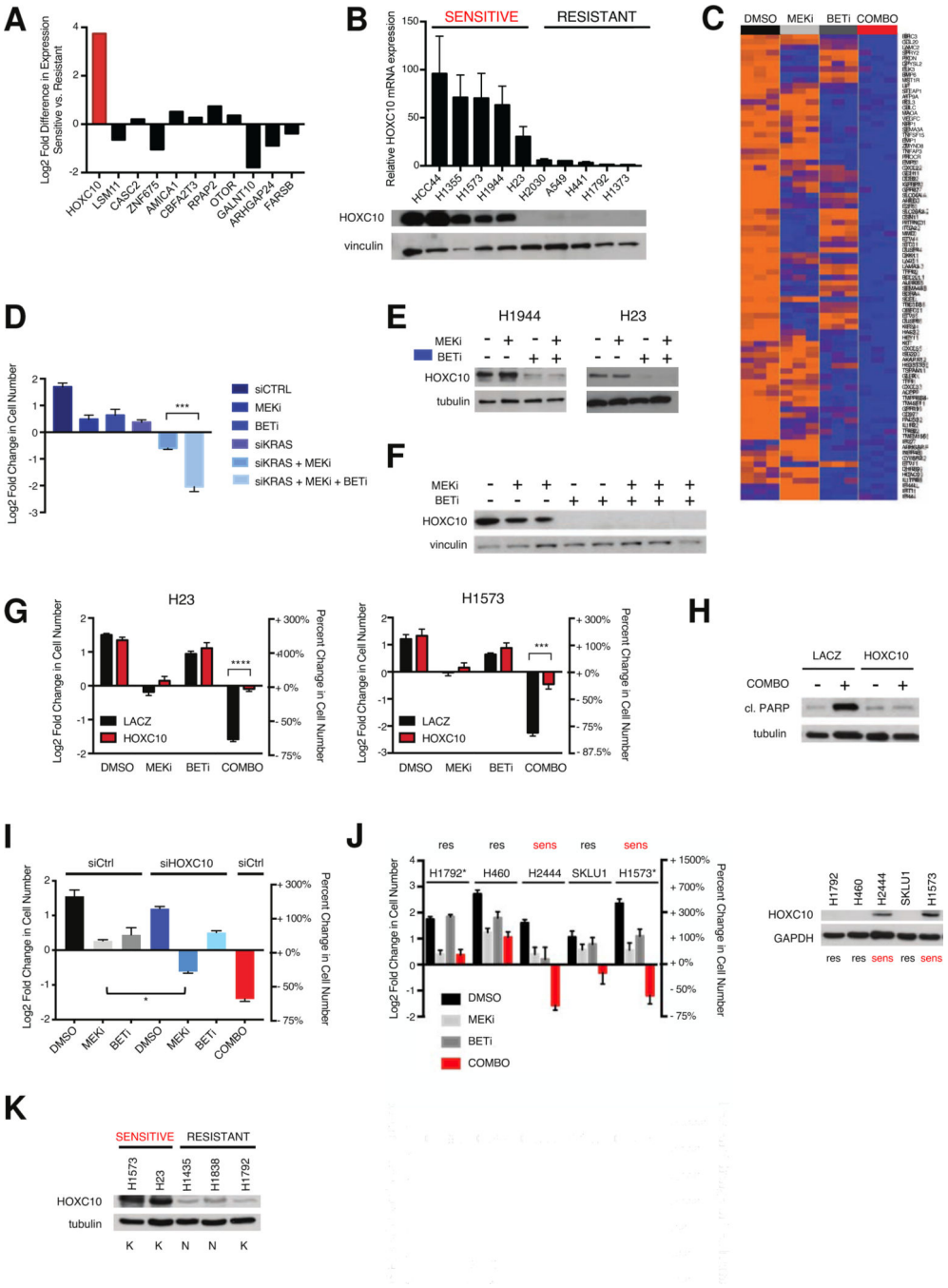

Figure 2. Identification of HOXC10 as a biomarker and mediator of sensitivity

(A) Transcript levels of genes differentially expressed between sensitive and resistant cell lines (CCLE; p<.001).

(B) *HOXC10* mRNA expression determined by qPCR (top, mean −/+ SD from technical triplicates) and corresponding immunoblot (bottom).

(C) Heatmap of RAS transcriptional output in H1573 cells after 24 hr treatments.

(D) Mean change in H1573 cell number −/+ SD from technical triplicates after 72 hr, determined by manual counting. ***p<0.0005 by two-tailed t-test with Welch's correction.

(E) HOXC10 protein expression in response to 24 hr treatments.
(F) HOXC10 immunoblot of H1573 xenografts.
(G) Change in cell number after 72 hr determined by manual counting of triplicate samples with or without ectopic HOXC10 (****p<0.0001).
(H) Cleaved PARP immunoblot in H1573 cells.
(I) Change in H23 cell number from triplicate samples after 72 hr (****p<0.0001, two-tailed t-test with Welch's correction)
(J) Change in cell number in triplicate samples after 72 hr treatments. Data from H1792 and H1573 cells are reproduced here from Fig. 1B, for comparison (*). ****p<0.0001 (Two-way Anova analysis and Tukey's post-hoc test) (left). HOXC10 immunoblot (right).
(K) HOXC10 immunoblot from *KRAS*-mutant "K" and *NF1*-mutant "N" cells.
See also Figure S3.

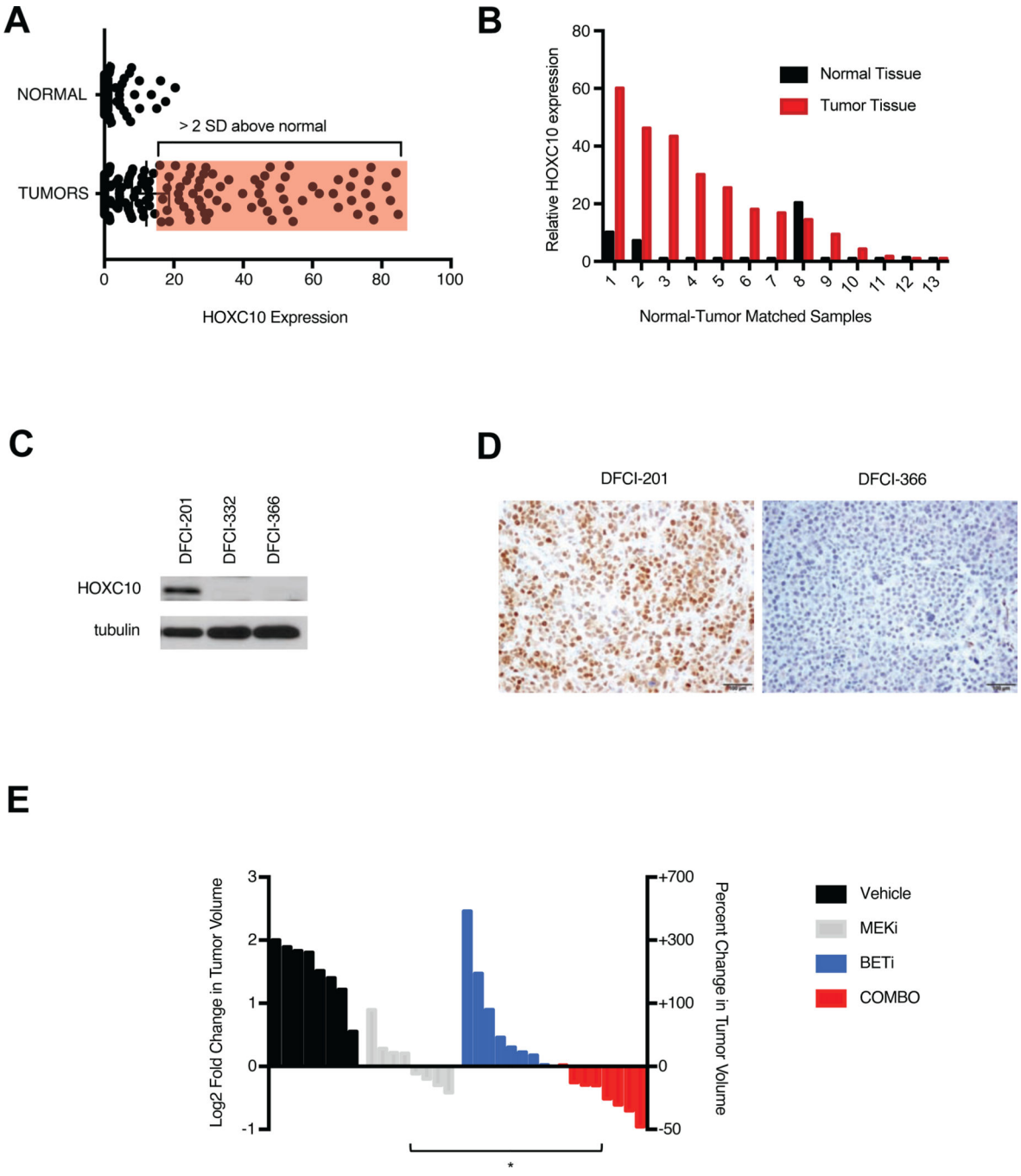

Figure 3. HOXC10 overexpression marks a distinct set of NSCLCs and a PDX model that is sensitive to MEK/BET inhibitors.

(A) *HOXC10* mRNA expression in normal lung and in *KRAS*-mutant lung adenocarcinoma (TCGA). Each dot represents a distinct sample. (Normal tissue n=58. Tumor tissue n=148).

(B) *HOXC10* mRNA expression of matched normal/tumor NSCLC samples. Data derived from the provisional TCGA data set. Expression normalized by HighSeq percentile (n=13).

(C) HOXC10 immunoblot of PDX samples.

(D) HOXC10 IHC of PDX tumors. Scale bar, 100 μM.

(E) Change in tumor volume of PDX DFCI-201 treated with the indicated drugs for 22 days, eight tumors per condition. *p=0.01 (2-tailed t-test)

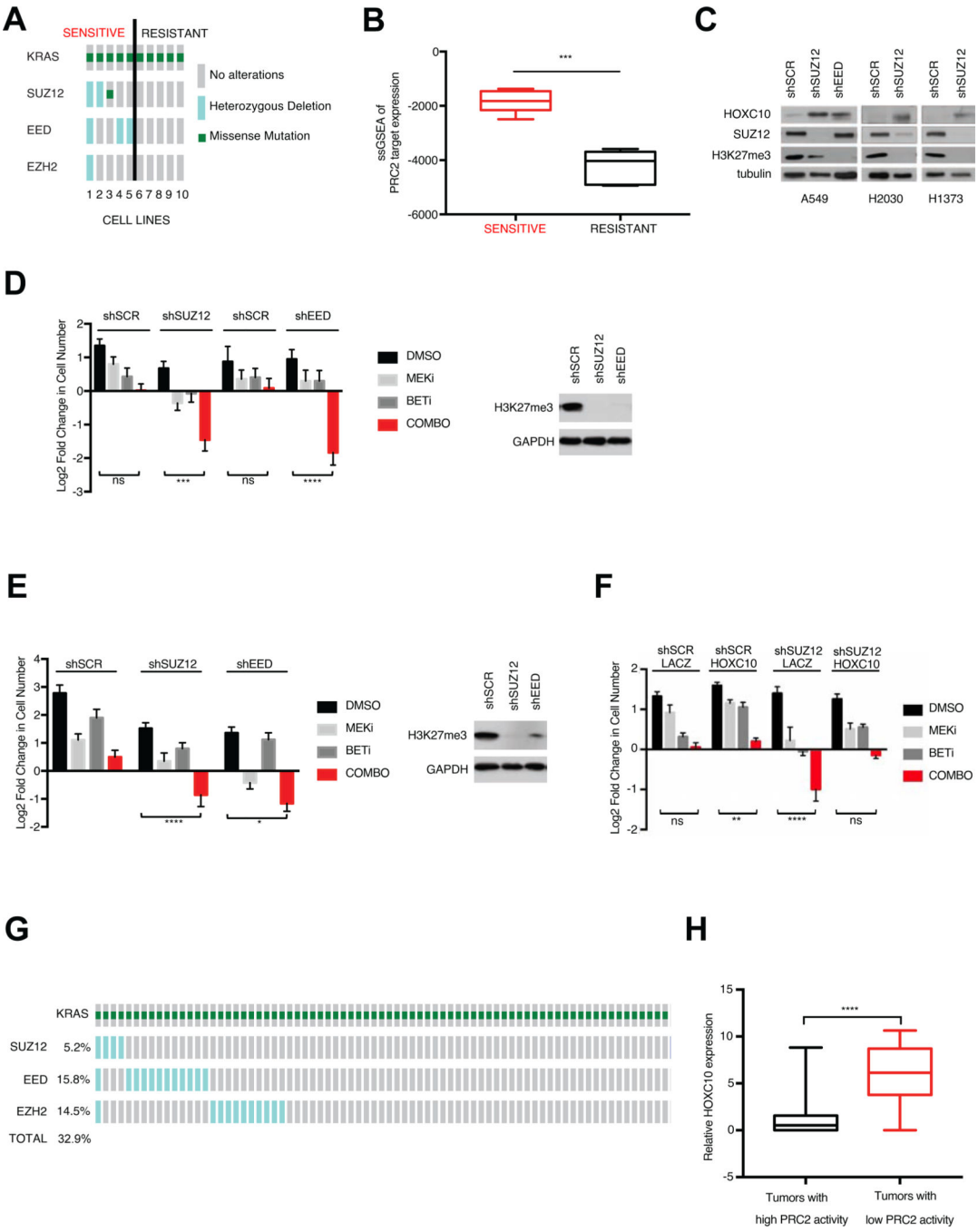

Figure 4. Defects in PRC2 trigger aberrant HOXC10 expression and confer sensitivity to combined MEK/BET inhibitors

(A) Oncoprint showing CNV loss and mutation of *SUZ12*, *EED*, and *EZH2* in cells: 1. H1573; 2. H1355; 3. H1944; 4. HCC-44; 5. H23; 6. H1373; 7. A549; 8. H441; 9. H1792; 10. H2030.

(B) Boxplot of ssGSEA analysis using CCLE data from cell lines in (A), comparing the expression of PRC2 targets. ***p<0.0005 (two-tailed t-test with Welch's correction).

Boxplots represent data within the 25th to 75th percentiles. Whiskers depict the range of all data points. Horizontal lines within boxes represent mean values.

(C) HOXC10 immunoblots. EED KD was confirmed by Q-PCR.

(D, E) Change in number of H2030 (D) or A549 (E) cells after 72 hr treatments, determined by manual counting. Mean −/+ SD from technical triplicates. Results are representative of ≥ 3 experiments. ****p<0.0001 (Two-way Anova analysis followed by Tukey's post-hoc test).

(F) Change in number of H2030 cells after 72 hr, determined by manual counting. Mean −/+ SD from technical triplicates. **p<0.001, ****p<0.0001 (Two-way Anova analysis followed by Tukey's post-hoc test)

(G) Oncoplot of CNV and mutational data of lung adenocarcinomas from TCGA 2014 dataset (n=75). Heterozygous loss (blue), mutations (green).

(H) Box plot of *HOXC10* expression in tumors with high versus low PRC2 activity (target expression). Boxplots represent data within the 25th to 75th percentiles. Whiskers depict the range of all data points. Horizontal lines within boxes represent mean values. ****p<0.0001 (two-tailed t-test with Welch's correction)

See also Figure S4.

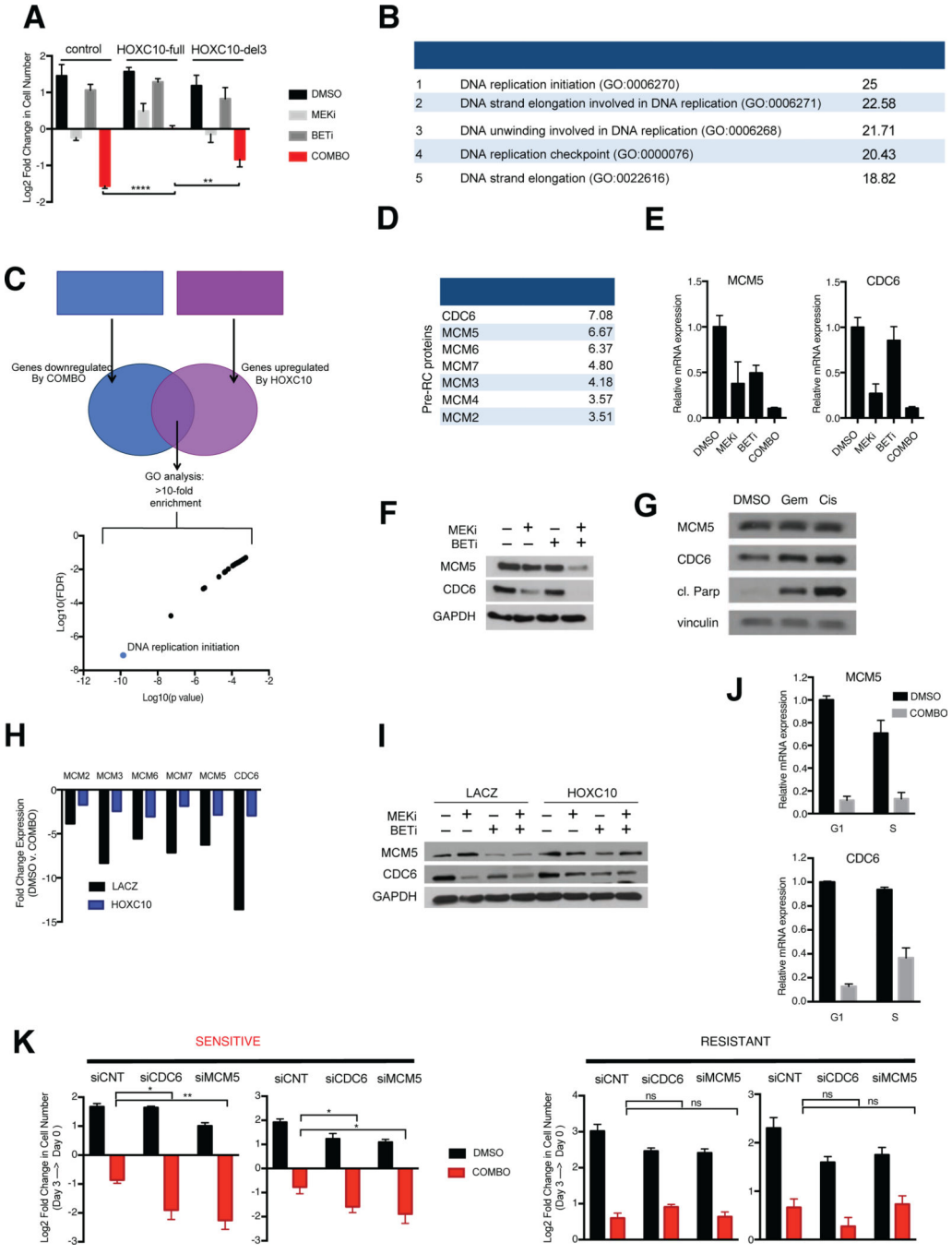

Figure 5. HOXC10 and MEK coordinately control the expression of pre-replication complex proteins

(A) Mean change in cell number (−/+ SD from technical triplicates) after 72 hr determined by manual counting. ****p<0.0001, **p<0.001.

(B) Table of results from GO analysis performed on genes significantly downregulated (fold change < −2, p< .001) in response to combination.

(C) Diagram depicting overlap of genes downregulated by combination and upregulated by ectopic HOXC10 expression (top). Graph depicting most significant lists (bottom).

(D) Table showing fold suppression of pre-RC complex genes in response to combination after 24 hr as determined by microarray.
(E) Mean expression of CDC6 and MCM5 mRNA, determined by qPCR in response to the indicated treatments, −/+ SD of three technical replicates.
(F) MCM5 and CDC6 immunoblots in H1573 cells.
(G) Immunoblots of MCM5, CDC6 and cleaved PARP in response to gemcitabine (Gem) or cisplatin (Cis) treatment (24 hr).
(H) Change in pre-RC gene expression in H1573 cells expressing LACZ or HOXC10 treated for 24 hr.
(I) Immunoblots of MCM5 and CDC6 in H1573 cells expressing LACZ or HOXC10.
(J) MCM5 and CDC6 mRNA expression in FACS sorted H1573 cells as determined by qPCR. Mean −/+ SD from technical triplicates.
(K) Effects of pre-RC suppression on cell number after 72 hr treatments, determined by manual cell counting. Sensitive cell lines (left, H23 and H1573). Resistant cells (right, H2030 and A549). Mean −/+ SD from technical triplicates. *$p<0.05$, **$p<0.01$, two-tailed t-test with Welch's correction.
See also Figure S5.

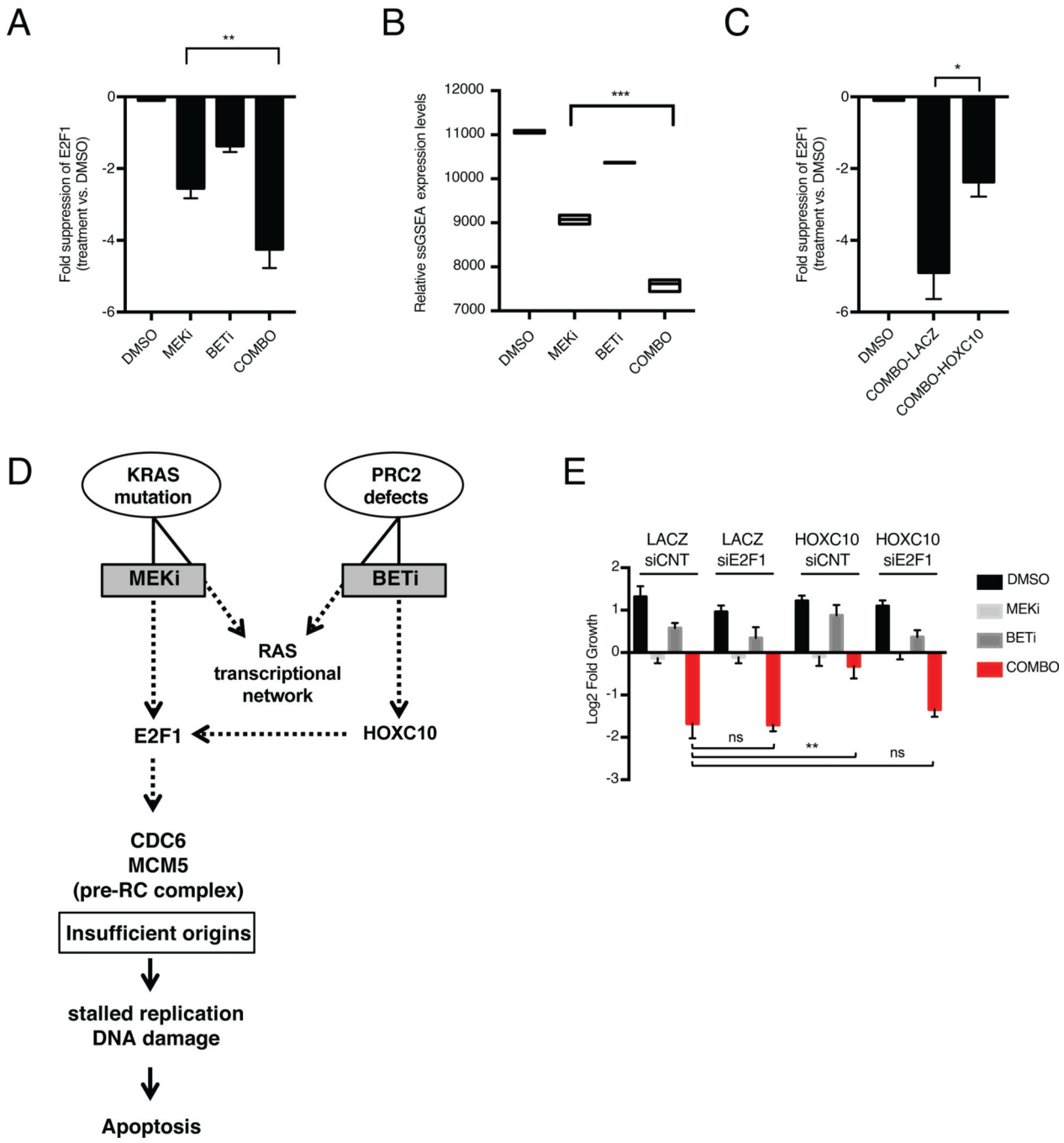

Figure 6. MEK and HOXC10 coordinately regulate pre-RC proteins via E2F1

(A) Mean fold suppression (−/+ SD from technical triplicates) of E2F1 mRNA in H1573 cells after 24 hr. **p = 0.0153, two-tailed t-test with Welch's correction.

(B) ssGSEA analysis of E2F1 target genes in H1573 cells after 24 hr. ***p = .0127 (two-tailed t-test with Welch's correction)

(C) Fold suppression of E2F1 in H1573 cells expressing ectopic LACZ or HOXC10. Mean −/+ SD from technical triplicates. *p = .0002 (two-tailed t-test with Welch's correction)

(D) Proposed mechanism of action of MEKi and BETi in lung cancer cells.

(E) Change in cell number of H1573 cells expressing LACZ or HOXC10 −/+ E2F1 siRNAs after 72 hr. Mean −/+ SD from technical triplicates. **p<0.01 (two-tailed t-test with Welch's correction)

See also Figure S6.

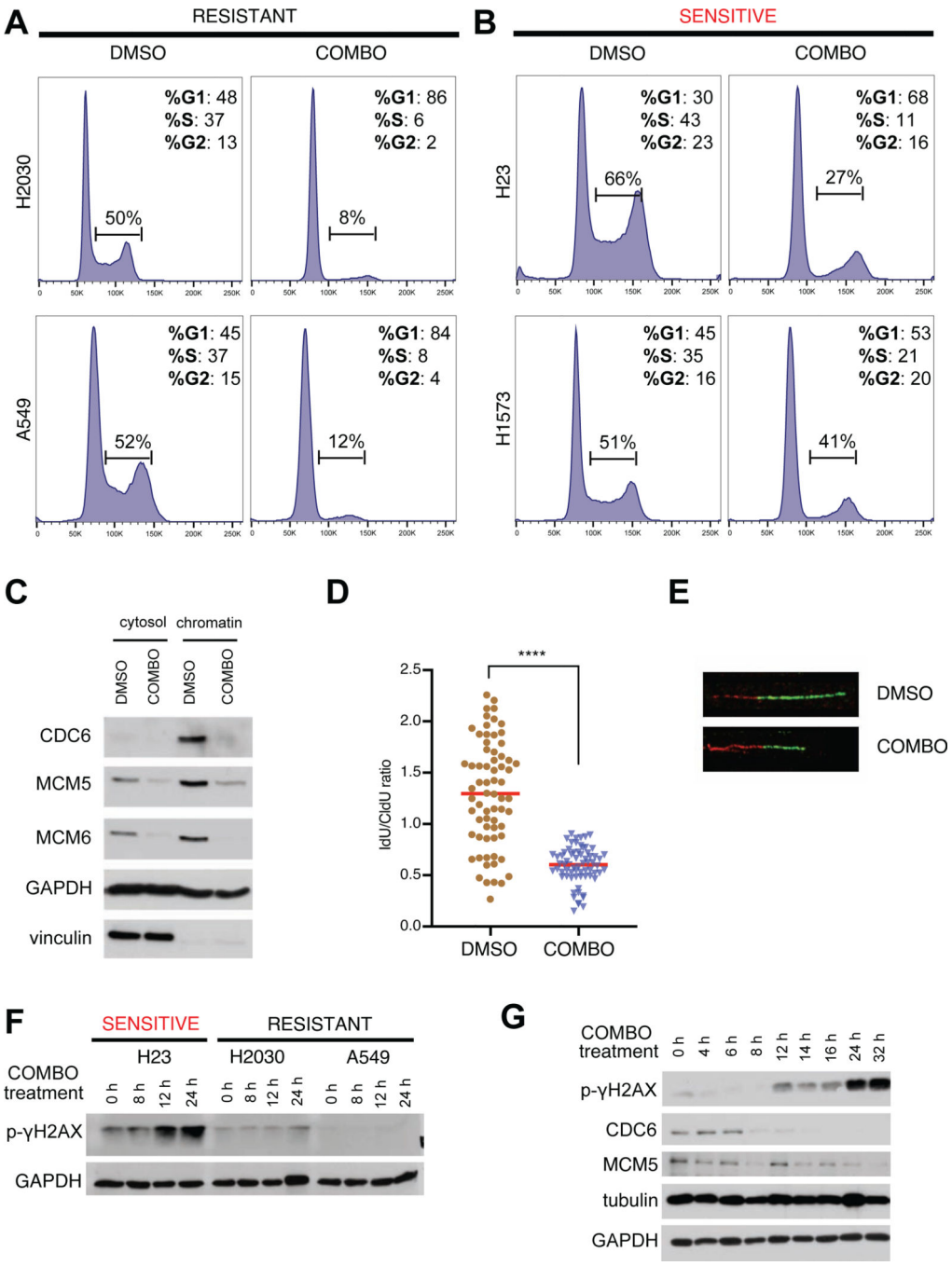

Figure 7. BET/MEK inhibitors kill HOXC10 expressing NSCLC by inducing replication fork stalling and DNA damage

(A,B) Cell cycle profiles of resistant (A) or sensitive (B) cells treated after 24 hr treatments.

(C) Immunoblots of cytosol and chromatin fractions of H1573 cells after 24 hr treatments.

(D,E) DNA fiber analysis (n=401 fibers) of H1573 cells treated with DMSO or MEK/BETi. Quantification of Idu/CIdU ratio (D) and image of representative fibers (E). Red represents CIdU labeling and green represents ldU labeling. ****p<0.0001, 2-tailed t-test.

(F) Phospho-γ-H2AX immunoblots. Results are representative of ≥3 biological replicates.

(G) Immunoblots of CDC6, MCM5 and phospho-γ-H2AX in sensitive H1573 cells. See also Figure S7.

KEY RESOURCES TABLE

REAGENT or RESOURCE	SOURCE	IDENTIFIER
Antibodies		
Anti-vinculin	Cell Signaling Technology	Cat# 4650, RRID:AB_10559207
Anti-H3K27me3	Cell Signaling Technology	Cat# 9733, RRID:AB_2616029
Anti-phospho-ERK	Cell Signaling Technology	Cat#4370; RRID:AB_2315112
Anti-GAPDH	Cell Signaling Technology	Cat# 2118, RRID:AB_561053
Anti-α-tubulin	Sigma Aldrich	Cat# T5168
Anti-HOXC10	AbCam	Cat# ab153904
Anti-SUZ12	Santa Cruz Biotechnology	Cat# sc-46264, RRID:AB_2196857)
Anti-MCM5	Santa Cruz Biotechnology	Cat# sc-165994, RRID:AB_2142526
Anti-CDC6	EMD Millipore	Cat# 05–550, RRID:AB_2276118
Anti-phospho-gamma-H2AX	Sigma Aldrich	Cat# # 05–636, RRID:AB_309864
Anti-c-MYC [Y69]	AbCam	Cat#ab32072, RRID:AB_731658
Anti-E2F1	Santa Cruz Biotechnology	Cat#sc-251, RRID:AB_627476
Anti-HA	Covance	Cat# MMS-101P-200, RRID:AB_10064068
Anti-beta tubulin	Sigma-Aldrich	Cat#T4026, RRID:AB_477577
Anti-cleaved PARP	CST	Cat#9541
Biological Samples		
DFCI-201; human KRAS-mutant NSCLC, female	Established at DFCI	N/A
DFCI-332; human KRAS-mutant NSCLC, male	Established at DFCI	N/A
DFCI-366; human KRAS-mutant NSCLC, male	Established at DFCI	N/A
Chemicals, Peptides, and Recombinant Proteins		
PD-0325901 (PD901, MEKi)	Gift from Kevin Shannon (UCSF)	N/A
JQ1 (BETi)	Shanghai Chempartner Co., Ltd China; large scale synthesis in collaboration with Jun Qi	N/A
Trametinib (MEKi)	LC Laboratories	CAS#871700–17-3
AZD5153 (BETi)	Chemietek	Cat# CT-A5153
Gemcitabine	Tocris	Cat# 3259
Cisplatin	Gift from Isaac Harris in the Brugge Lab	
Critical Commercial Assays		
Lipofectamine RNAiMAX	ThermoFisher Scientific	Cat#13778030
IncuCyte caspase3/7 apoptosis assay reagent	IncuCyte	Cat# 4440
IncuCyte Nuclight red (mKate2) reagent	IncuCyte	Cat# 4476
Affymetrix GeneChip Human Gene 2.0 ST array chip	ThermoFisher Scientific	Cat#902499
Qiagen RNeasy kit	Qiagen	Cat#74104
Hoechst 33342 Staining Dye Solution	Abcam	Cat# ab228551, RRID:AB_2651135

REAGENT or RESOURCE	SOURCE	IDENTIFIER
Deposited Data		
Microarray data of NCI-H1573 cell line treated with DMSO, MEKi, BETi, and COMBO after 24 hours	Gene Expression Omnibus	Accession #: GSE118903, SuperSeries # GSE118909
Microarray data of NCI-H1573+ LACZ and H1573+ HOXC10 treated with DMSO and Combined MEKi and BETi	Gene Expression Omnibus	Accession #: GSE118908, SuperSeries # GSE118909
Experimental Models: Cell Lines		
A-549	ATCC	ATCC Cat# CRL-7909, RRID:CVCL_0023
HCC44	Gift from William Hahn lab (DFCI)	RRID:CVCL_2060
NCI-H2444	ATCC	ATCC Cat# CRL-5945, RRID:CVCL_1552
NCI-H1355	ATCC	ATCC Cat# CRL-5865, RRID:CVCL_1464
NCI-H1373	ATCC	ATCC Cat# CRL-5866, RRID:CVCL_1465
NCI-H1435	ATCC	ATCC Cat# CRL-5870, RRID:CVCL_1470
NCI-H1573	ATCC	ATCC Cat# CRL-5877, RRID:CVCL_1478
NCI-H1792	ATCC	ATCC Cat# CRL-5895, RRID:CVCL_1495
NCI-H1838	ATCC	ATCC Cat# CRL-5899, RRID:CVCL_1499
NCI-H1944	ATCC	ATCC Cat# CRL-5907, RRID:CVCL_1508
NCI-H2030	ATCC	ATCC Cat# CRL-5914, RRID:CVCL_1517
NCI-H23	ATCC	ATCC Cat# CRL-5800, RRID:CVCL_1547
NCI-H441	ATCC	ATCC Cat# CRM-HTB-174, RRID:CVCL_1561
NCI-H460	Gift from William Hahn lab (DFCI)	RRID:CVCL_0459
SK-LU-1	ATCC	ATCC Cat# HTB-57, RRID:CVCL_0629
Experimental Models: Organisms/Strains		
Mouse: Nu/Nu laboratory mice for cell line-derived xenograft models	Charles River Laboratories	RRID:IMSR_CRL:088
Mouse: NOD-scid (NSG) laboratory mice for PDX model	The Jackson Laboratory	RRID:IMSR_JAX:005557
Oligonucleotides		
Human KRAS ON-TARGET SMARTpools siRNA	Dharmacon	Cat# L-005069–00-0005
Human CDC6 ON-TARGET SMARTpools siRNA	Dharmacon	Cat# L-003233–00-0005
Human MCM5 ON-TARGET SMARTpools siRNA	Dharmacon	Cat# L-003276–00-0005
Human E2F1 ON-TARGET SMARTpools siRNA	Dharmacon	Cat# L-003259–00-0005
MCM5-forward (5′–3′): AGCATTCGTAGCCTGAAGTCG	Invitrogen	N/A
MCM5-reverse (5′–3′): CGGCACTGGATAGAGATGCG	Invitrogen	N/A
CDC6-forward (5′–3′): GACCTCAAGAAGGAACTG	Invitrogen	N/A

REAGENT or RESOURCE	SOURCE	IDENTIFIER
CDC6-reverse (5′–3′): ATACCTCTTCCTGACAAATCTC	Invitrogen	N/A
HOXC10-forward (5′–3′): CTATCCGTCCTACCTCTCGCA	Invitrogen	N/A
HOXC10-reverse (5′–3′): ACATGCAGCAGACATTCTCCT	Invitrogen	N/A
GAPDH-forward (5′–3′): GCCGGCTCCGTTATGG	Invitrogen	N/A
GAPDH-reverse (5′–3′): AACCTGGTTCATCATCACTA	Invitrogen	N/A
UBC-forward (5′–3′): GCCGGCTCCGTTATGG	Invitrogen	N/A
UBC-reverse (5′–3′): AACCTGGTTCATCATCACTA	Invitrogen	N/A
Recombinant DNA		
HOXC10 pHAGE HA-FLAG-C-terminal	Harvard PlasmID Database	Cat#HsCD00453850
pHAGE LACZ HA-FLAG-N-terminal	Backbone was gift from Wader Harper and LACZ cloned in (McLaughlin et al, 2013)	N/A
HOXC10-full-pHAGE-PGK-FLAG-HA-GAW-IRES-PURO-N-terminal	Gift from Elledge lab (Brigham and Women's Hospital)	N/A
HOXC10-homebox deletion-pHAGE-PGK-FLAG-HA-GAW-IRES-PURO-N-terminal	Gift from Elledge lab (Brigham and Women's Hospital)	N/A
shSUZ12- target sequence 5′-GCTGACAATCAAATGAATCAT-3	RNAi consortium of the Broad Institute	NM_015355.1–2076s1c1
Software and Algorithms		
GraphPad PRISM 7.0	GraphPad	RRID:SCR_002798
BRBArrayTools Version 4.5.1 plug-in in Microsoft Excel 2016	Biometric Research Program, National Cancer Institute	RRID:SCR_000778
GSEA: Gene Set Enrichment Analysis software	Broad Institute	RRID:SCR_003199
GenePattern ssGSEAProjection	Broad Institute	RRID:SCR_003201
cBioPortal for Cancer Genomics visualizer	Memorial Sloan Kettering	RRID:SCR_014555
Gene Ontology	Gene Ontology Consortium	RRID:SCR_006941
FlowJo	FlowJo, LLC	RRID:SCR_008520
Gene Expression Omnibus	NCBI	RRID:SCR_005012